Packed Bed Column Adsorption of Phenol Onto Corn Cob Activated Carbon: Linear and Nonlinear Kinetics Modeling

Christopher Chiedozie Obi (oc.christopher@unizik.edu.ng)
Nnamdi Azikiwe University Faculty of Engineering Technology https://orcid.org/0000-0002-8654-1240
Chamberlain Ositadinma Iheanacho
Nnamdi Azikiwe University
Joseph Tagbo Nwabanne
Nnamdi Azikiwe University
Chijioke Elijah Onu
Nnamdi Azikiwe University

Research

Keywords: Corn cob, Activated carbon, Phenol, Packed bed column, Linear and nonlinear models

Posted Date: December 4th, 2020

DOI: https://doi.org/10.21203/rs.3.rs-117100/v1

Manuscript Title:

Packed Bed Column Adsorption of Phenol onto Corn Cob Activated Carbon: Linear and Nonlinear Kinetics Modeling

Authors' Names:

[1]Christopher Chiedozie Obi

[2]Ositadinma Chamberlain Iheanacho

[3]Joseph Tagbo Nwabanne

[4]Chijioke Elijah Onu

Authors' Institution:

[1,2,3,4]Department of Chemical Engineering, Nnamdi Azikiwe University, P.M.B. 5025 Awka, Anambra State, Nigeria.

Corresponding Author's E-mail:

oc.christopher@unizik.edu.ng

Corresponding Author's ORCID:

https://orcid.org/0000-0002-8654-1240

Abstract

In the present study, linear and nonlinear regression analysis for packed bed column adsorption of phenol onto corn cob activated carbon was investigated. The activation of the corn cob provided the activated carbon with enhanced surface area and micropore volume of 903.7m^2/g and 0.389 cm^3/g respectively. The analysis of the physical properties of the corn cob activated carbon (CCAC) revealed that it contained 33.47% of fixed carbon. SEM images indicated the presence of interspatial pores within the matrix of the adsorbent, while the FTIR analysis revealed that the major functional groups in CCAC were alkanol, alkanes, alkyls, carboxylic acids, ethers, esters, and nitro compounds. The effect of the process parameters influencing the dynamic adsorption process was investigated at flow rates (9 – 18mg/min), initial phenol concentration (100-300mg/l), bed height (5 – 10cm), and particle size (300-800µm). Breakthrough time and adsorption capacity increased with an increase in bed height but decreased with an increase in flow rate, initial phenol concentration, and particle size. At 9mg/min flow rate, 100mg/l initial phenol concentration, 10 cm bed height, and 300µm, the breakthrough and saturation points adsorption capacities were 2.143 and 8.570 mg/g respectively, the volume of effluent treated at saturation point was 12.96L, the length of mass transfer zone (MTZ) was 7.50cm, while 66.13% phenol removal efficiency was achieved. The linear and nonlinear regression analysis of the dynamic column adsorption models viz. Thomas, Adam Bohart, and Wolborska fitted better with the experimental data as compared to Yoon–Nelson. Generally, the nonlinear regression analysis proved to be a better tool for dynamic adsorption model analysis because the model parameters it predicted are in higher proximity to the experimental data when compared to those obtained via linear regression analysis. Conclusively, this study has shown that CCAC can successfully be used for the removal of phenol from aqueous solutions. It also provided experimental evidence that for a more accurate analysis of dynamic adsorption models nonlinear regression tool should be considered.

Keywords: Corn cob, Activated carbon, Phenol, Packed bed column, Linear and nonlinear models.

1. Introduction

Policymakers and researchers have recently become more concerned about the effects of human and aquatic life exposure to chemical compounds in the environment. Among the major chemicals of great concern are phenol and phenolic compounds. This is because phenol and phenolic compounds are renowned to be toxic and have short and

long term consequences on humans and animals [1]. Phenol is very dangerous, harmful, and causes excretion of dark urine, impaired vision, diarrhea, and sour mouth [2]. The major industries producing phenol contaminated effluents are the chemical and pharmaceutical industries. Other industries associated with such effluents are resin manufacturing industries, coal gasification operating units, pulp and paper mills, liquefaction processing units, dye synthesis units, petroleum refineries, and petrochemical industries [2, 3]. There is increased awareness of the need to remove these contaminant from industrial effluents before they are discharged.

There are many wastewater treatment techniques available for the removal of phenol from industrial effluents. The most common techniques include membrane separator, ion exchange, steam stripping, solvent extraction, hot gases, solar photo-catalytic system, photodecomposition, volatilization, and adsorption, as well as biological methods [2, 4-7]. Adsorption is widely considered an efficient technique for the decontamination of industrial effluents. The preference for adsorption is mostly because it is less expensive in terms of design, land space, and operating cost and more efficient in comparison with other processes [8, 9]. The performance of the adsorption process majorly depends on the characteristics of the adsorbent such as micro-porous structure, surface area, surface reactivity, and adsorption capacity, as well as the operating conditions.

Batch and column (dynamic) operations are the major techniques by which the contact between the adsorbate and the adsorbent is achieved in the adsorption process. However, the packed bed column is often preferred for the removal of various contaminations from industrial effluents because of its operational simplicity, high pollutant removal efficiency, and ease of scale-up from a laboratory process. To successfully design and operate a packed bed adsorption process, the breakthrough curves must be predictable under defined operating conditions [9, 10]. The breakthrough curve is a representation of the loading behavior of the target pollutant onto the adsorbent in a continuous column adsorption process. It is described as the ratio of pollutant concentration to influent concentration as a function of time or volume of effluent for a given bed height [9, 11].

Activated carbon is the most commonly used adsorbent for the adsorption of wastewater pollutants. Activated carbon is often preferred due to its high affinity for pollutants in wastewater majorly because of its high surface area, microporous structure, high adsorption capacity, and a high degree of surface reactivity. The high cost of commercial

activated carbon makes research on the synthesis of activated carbon from various agricultural waste materials valuable. Various agricultural materials have been investigated for the preparation of activated carbon for pollutants removal from wastewater. The most commonly reported ones are rice husk [12-14], wheat bran [15-17], fly ash [18-20], cashew nutshell [21], water hyacinth ash [22], sawdust [23, 24], soybean shell [14, 25], eggshell [26, 27], medlar seed [28] coconut shell [29, 30], palm kernel shell [31, 32], and corn cob [14].

Also, some agro-waste materials have been investigated for phenol removal from simulated and industrial wastewater, these include eggshell [26], rice straw and onion dry scales [33], wheat bran [34], olive mill waste [35], palm kernel shell [36], deoiled soya [37], Black Gram Husk (BGH), Green Gram Husk (GGH), and Rice Husk [38], oil palm empty fruit bunches [39].

Corn cob is a waste product generated during corn processing. It is the frame-like part of the maize plant on which the yellow maize seeds grow. Corn cob is considered a waste material because when the maize that is considered valuable is detached, the cob is usually discarded as waste. Hence, millions of tons of corn cob are dumped as waste annually, constituting environmental pollution. It was reported by Gireiet al. [40] that Nigeria produced about 10.5 million metric tons of maize in 2016/2017. Finding an economic utilization of this agro-waste is a valuable research exercise. The application of corn cob activated carbon in the removal of some wastewater pollutants have been investigated and reported by some researchers, mercury [41], uranium [8], chromium [Cr(III) and Cr(VI)] [42], nitrogen dioxide and hydrogen sulphide [43], and arsenic [44]. No report is available in the open literature on the use of corn cob activated carbon for the decontamination of phenol contaminated effluent in a dynamic adsorption system.

Linear regression is the most commonly applied method for evaluating the fitting correlation quantifying the distribution of adsorbates on the surface of adsorbents, and validating the consistency of an adsorption model in predicting the outcome of an adsorption process. Most authors have reported the application of a linear regression tool for kinetics of column adsorption analysis [8-10, 45]. However, with the advancement in the use of computer technology in the analysis of scientific data, the application of nonlinear regression tool in adsorption kinetic modeling exercise has been expedited. In contrast to linear regression analysis, nonlinear regression analysis is typically concerned with the minimization or maximization of the error distribution between the experimental data and the

model predicted data. With regard to information available in the open literature, it is worthy of note that the nonlinear approach to model analysis for column adsorption process has not been given quality attention by researchers. Hanet al. [46] compared linear and nonlinear analysis of methylene blue adsorption onto natural zeolite in a column adsorption system but only Thomas model was considered by the authors. Since there are several models that could be used to analyze a column adsorption system, the information presented by the authors was insufficient to give a deep understanding of the impact of the modeling approach on column adsorption systems especially when the analysis of other models are considered. Nonlinear analysis of the dynamic models of phenol removal using corn cob activated carbon has not been reported.

In the present study, activated carbon was prepared from corn cob and the adsorption performance of the prepared adsorbent was evaluated for phenol removal in a packed bed column. The effects of various process variables such as flow rate, influent phenol concentrations, bed height, and particle size on breakthrough curves were investigated. Other parameters needed for the successful design of packed bed adsorption column for large scale application of the process such as adsorption capacity at breakthrough and saturation points, adsorption efficiency at saturation point, length of the Mass Transfer Zone (MTZ), amount of phenol loaded in the column and the volume of effluent treated at saturation points were computed and presented in this report. With the aid of Microsoft Excel's Solver Extension software program, various kinetic parameters of the column experimental data were estimated using a nonlinear regression tool and compared with the linear regression result.

2. Materials and Experimental Procedure

2.1 Raw materials

The raw corn cob sample was obtained from a local maize farm at Okpuno, Awka, Nigeria. Distilled water, tetraoxophosphoric acid (H_3PO_4), Phenol, and other reagents were purchased from Chemicals and Reagents market in Onitsha, Nigeria. All reagents used in the experiments were of analytical grade.

2.2 Preparation of the Adsorbate

A stock solution of phenol was prepared by dissolving a measured amount of phenol in distilled water. Concentrations of 100mg/l, 200mg/l, and 300mg/l were prepared and used for the packed bed column experiments.

131 **2.3 Preparation and Characterization of the Adsorbent**

132 The raw corn cob sample was first washed with tap water to remove associated impurities, and then with distilled
133 water. The relatively purified sample was sun-dried, crushed, and again sun-dried to further eliminate associated
134 moisture. The sample was activated with a 45% concentration of tetraoxophosphuric acid, H_3PO_4, and kept in an oven
135 at 110^{o}C for 24 hours. Thereafter, the activated sample was washed with deionized water until a pH of 7 was obtained.
136 The carbonization of the activated corn cob sample was carried out in a muffle furnace at a carbonization temperature
137 of 575^{o}C for 4 hours. The CCAC sample was soaked in distilled water and recovered by filtration. The recovered
138 CCAC was dried in an oven at 110^{o}C for 24 hours, ground, sieved to obtain particle sizes of 300 μm, 600 μm, and 800
139 μm, and stored in an airtight container before use.
140
141 The physical properties of the activated carbon were determined following standard methods of the Association of
142 Official Analytical Chemists [47]. pH was measured using a pH meter (Elico model L1 -120). The surface area and
143 the pore volume were determined using the BET nitrogen (N_2) adsorption-desorption isotherms measured at 77K using
144 N_2 gas sorption analyzer as described by Sivakumaret al. [48]. The surface areas were calculated via the nitrogen
145 adsorption isotherms on the assumption that the surface area of a nitrogen molecule is 0.162 nm^2. The instrumental
146 analysis of the raw and the activated corn cob samples was carried out via Fourier Transform Infrared (FTIR)
147 spectrophotometer and Scanning Electron Microscope (SEM). A Shimadzu FTIR-8400S model was used for the
148 determination of the functional groups inherent in the samples. The surface morphology of the samples was determined
149 with the aid of a Joel scanning electron microscope (model, JSM 6400). The micrograph of CCAC was done at 500x
150 and 1000x magnifications for the adsorbents sieved at 300μm.
151

152 **2.4 Column Adsorption Studies**

153 The packed bed column experiments were performed with the aid of a glass column of 30cm high and 30mm internal
154 diameter. The schematic diagram of the column adsorption system is shown in Fig. 1. The phenol solution was pumped
155 into the column with the aid of a peristaltic pump (BQ 50-IJ-A) as shown in Fig 1. With the aid of a flow controller,
156 the flow rate was regulated. The CCAC adsorbent was packed in the column with glass wool at the bottom of the
157 column to avoid the loss of adsorbent during the continuous operation process. The shape of the breakthrough curves
158 was studied at different operating conditions by collecting samples at different time intervals of 1 hour up to 24 hours

until the adsorbents became saturated. The experimental data were further subjected to linear and nonlinear regression analysis of Thomas, Yoon Nelson, Adam-Bohart, and Wolborska kinetic models to determine the fitness of the experimental data to the models.

The various process variables at which the column study was carried out are flow rates (9ml/min, 13ml/min, and 18ml/min), influent phenol concentrations (100mg/l, 200mg/l and 300mg/l), packing height (5cm, 7.5cm, and 10cm) and particle size (300 µm, 600 µm, and 800 µm).

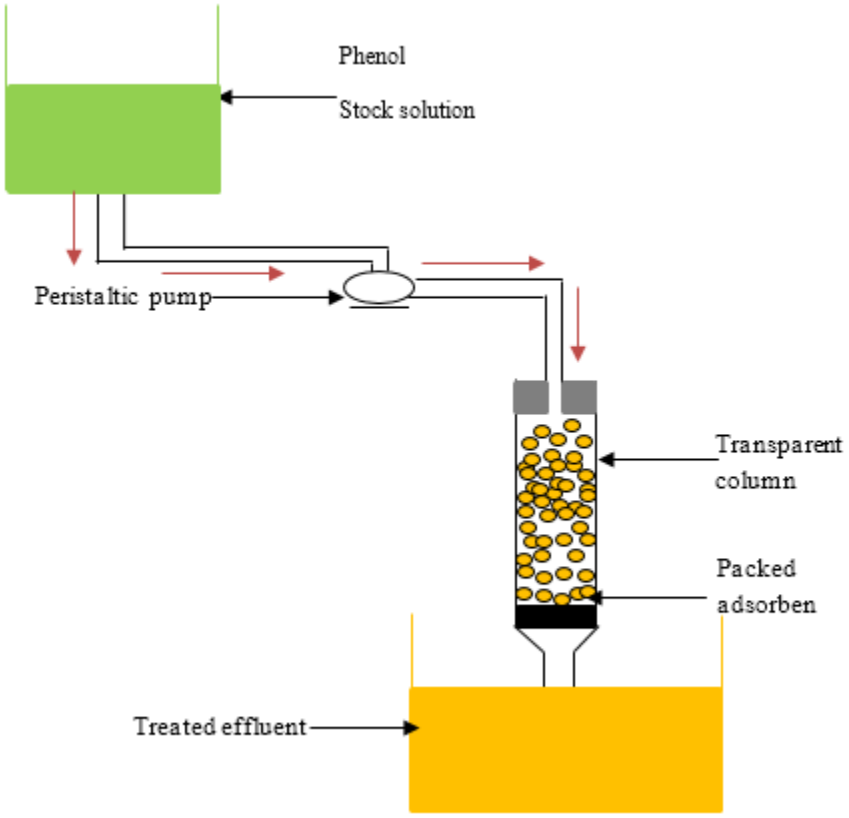

Fig. 1 Packed bed column experimental set up

2.5 Estimation of the adsorption column design parameters

Certain parameters are key to the design of a dynamic packed bed adsorption system for large scale application. Amongst the necessary design parameters are the adsorption capacity at breakthrough and saturation points. These are determined using Eqs. (1) and (2) [49]:

$$q_b = \frac{C_o Q}{m} \int_0^{t_b} \left(1 - \frac{C}{C_o}\right) dt \quad (1)$$

$$q_s \frac{C_o Q}{m} \int_0^{t_s} \left(1 - \frac{C}{C_o}\right) dt \quad (2)$$

Where q_b is the adsorption capacity at breakthrough time (mg/g), q_s is the adsorption capacity at saturation, also denoted as q_e representing equilibrium adsorption capacity (mg/g), m is the mass of adsorbent (g), Q is the volumetric flow rate (mL/min), C_o is the initial phenol concentration (mg/mL), C is the concentration of phenol at a time t, (mg/mL), t_b is the breakthrough time (min) and t_s is the saturation time (min).

The percentage removal of phenol at saturation (Y) is determined by calculating the amount of phenol loaded in the column, the amount of unadsorbed phenol and the amount of phenol adsorbed at saturation [50];

The amount of phenol that was loaded in the column at saturation ($m_{in,s}$, mg) is giving by Eq. (3):

$$m_{in,s} = C_o Q t_s \quad (3)$$

The amount of phenol ($m_{out,s}$, mg) that left the column unadsorbed at saturation is given by Eq. (4):

$$m_{out,s} = C_o Q \int_0^{t_s} \left(\frac{C}{C_o}\right) dt \quad (4)$$

The amount of phenol adsorbed in the column ($m_{ads,s}, mg$) at saturation is given by Eq. (5):

$$m_{ads,s} = m_{in,s} - m_{out,s} \quad (5)$$

The percentage removal at saturation is given by Eq. (6):

$$Y_s(\%) = \frac{m_{ads,s}}{m_{in,s}} \times 100 \quad (6)$$

The length of the Mass Transfer Zone (MTZ, cm) is calculated using Eq. (7) [49]:

$$MTZ = Z\left(1 - \frac{q_b}{q_s}\right) \quad (7)$$

While the volume of the effluent treated ($V_{eff,s}$, L) at saturation point is given by Eq. (8):

$$V_{eff,s} = Q t_s \quad (8)$$

Where Z is the height of the bed (cm). The other variables are as defined initially.

2.6 Dynamic adsorption kinetics models used in the study

In the industrial usage of adsorbents, the time dependence of adsorption on solid surfaces is termed adsorption kinetics [51]. In the present study, the experimental data were subjected to four adsorption kinetics models, viz. Wolborska, Yoon Nelson, Adam-Bohart, and Thomas. The linear form of the model equations, the plots made, and the model parameters are presented in Table 1 while the nonlinear forms of the models are presented in Table 2.

Table 1 Linear column kinetic model equations

Model	**Equation**	**Eq. No.**	**Plot**	**Model Parameter**	**Source**
Thomas	$\ln\left(\frac{C_t}{C_o} - 1\right) = \frac{K_{TH} q_e m}{Q} - K_{TH} C_o t$	9	$\ln\left(\frac{C_o}{C_t} - 1\right)$ vs t	K_{TH} q_e	[9]
Adam-Bohart	$\ln\frac{C_t}{C_o} = K_{AB} C_o t - K_{AB} N_o \frac{Z}{U_o}$	10	$\ln\frac{C_t}{C_o}$ vs t	K_{AB} N_o	[52]
Wolborska	$\ln\frac{C_t}{C_o} = \frac{\beta C_o}{N_o} t - \frac{\beta Z}{U_o}$	11	$\ln\frac{C_t}{C_o}$ vs t	β N_o	[9]
Yoon Nelson	$\ln\left(\frac{C_t}{C_o - C_t}\right) = K_{YN} t - \tau K_{YN}$	12	$\ln\left(\frac{C_t}{C_o - C_t}\right)$ vs t	K_{YN} τ	[9]

Table 2 Nonlinear column kinetic model equations

Model	Equation	Eq. No.	Model Parameter	Source
Thomas	$\frac{C_t}{C_o} = \frac{1}{1 + exp\left[\frac{K_{TH}(q_{TH}m - C_0V)}{Q}\right]}$	13	K_{TH} q_e	[52]
Adam-Bohart	$\frac{C_t}{C_o} = exp\left(K_{AB}C_o t - K_{AB}N_o\frac{Z}{U_o}\right)$	14	K_{AB} N_o	[52]
Wolborska	$\frac{C_t}{C_o} = exp\left(\frac{\beta C_o t}{N_o} - \frac{\beta Z}{U_o}\right)$	15	β N_o	[52]
Yoon Nelson	$\frac{C_t}{C_o} - C_t = exp(K_{YN}t - K_{YN}\tau)$	16	K_{YN} τ	[52]

2.7 Error analysis

The fitness of the different mathematical models to the experimental data and the error distribution in the prediction of the model parameters were assessed using various error functions viz. Root Mean Square Error (RMSE), Chi-square function (χ^2), Sum of Squares Errors (SSE), Sum of Absolute Errors (SAE), and the Average Relative Errors (ARE), as well as the coefficient of determination (R^2). The error functions are presented in Table 3.

Table 3 The mathematical expressions of the error functions.

Error Function	Abbreviation	Expression	Eq. No.	Source
Coefficient of determination	R^2	$1-\frac{\sum_{i=1}^{N}\left(q_{e,exp}-q_{e,pred}\right)^2}{\sum_{i=1}^{N}\left(q_{e,exp}-\overline{q_{e,exp}}\right)^2}$	17	[53]
Root Mean Square Error	RMSE	$\sqrt{\frac{1}{\mathrm{N}-2}\sum_{i=1}^{N}\left(q_{e,exp}-q_{e,pred}\right)^2}$	18	[54]
Chi-square function	χ^2	$\sum_{\mathrm{i=1}}^{\mathrm{N}}\left[\frac{\left(\mathrm{q_{e,exp}}-\mathrm{q_{e,pred}}\right)^2}{\mathrm{q_{e,exp}}}\right]$	20	[55]
Sum of Squares Errors	SSE	$\sum_{i=1}^{N}\left(q_{e,exp}-q_{e,pred}\right)^2$	21	[53]
Sum of Absolute Errors	SAE	$\sum_{i=1}^{N}\left(q_{e,exp}-q_{e,pred}\right)$	22	[56]
Average Relative Errors	ARE	$\frac{100}{N}\sum_{i=1}^{N}\left(\frac{q_{e,exp}-q_{e,pred}}{q_{e,exp}}\right)$	23	[53]

The subscripts "exp" and 'pred" represent the experimental and predicted values and *N* is the number of observations in the experimental data.

3. Results and discussion

3.1 Characterization of the adsorbent

3.1.1 Physical properties, BET surface area, and pore size distribution of the adsorbent

The physical properties of CCAC are presented in Table 4. The physical properties of the adsorbent considered include bulk density, pH, ash content, iodine number, moisture content, porosity, volatile matter, and fixed carbon. The data shows that CCAC has low values of moisture content (5.5%), percentage of volatile matter (18.01%), ash content (5.82%), and moderate content of fixed carbon (33.47%). When the volatile matter content is high, the solid yield in the carbonization stage is reduced. An iodine number of 888.34.84 was obtained. The iodine number is used as an index to investigate the internal structure and surface area of the activated carbon [57]. Shanmugamet al. [58] noted that the carbonization and activation process conditions are not the only major contribution towards the porous structure of activated carbon but also being influenced by the original nature and structure of the starting material.

Similarly, the BET surface area, pore width, micropore volume, pore radius as well as adsorption energy are presented in Table 5. The results provide qualitative information on the pore structure of the produced activated carbon. The surface area of an adsorbent is one of its most significant property that determines its sorption capacity. The surface area is quite high (903.7m^2/g), this affirms that CCAC is a good adsorbent for the sorption of adsorbates. The adsorption energy is relatively moderate, a value of 4.68KJ/mol was obtained.

Table 4 Physical properties of CCAC

Property	**CCAC**
Bulk density (g/ml)	0.625
pH	6.3
Ash content (%)	5.82
Iodine Number (mg/g)	888.34.84
Moisture content (%)	5.5
Porosity (η)	0.235
Volatile matter (%)	18.01
Fixed Carbon (%)	33.47

Table 5 BET surface area and pore size distribution of CCAC

Property	CCAC
Multipoint BET surface area (m^2/g)	903.7
Average pore width (nm)	5.55
Micropore volume (cm^3/g)	0.389
Adsorption energy (KJ/mol)	4.68
Pore radius (A^o)	16.20

3.1.2 Instrumental Analysis

The SEM images of the raw corn cob and CCAC at 500x and 1000x magnification are presented in Fig. 2(a), 2(b), and 2(c) respectively. The morphology of the raw sample (Fig. 2(a)) has a curled and highly packed surface with non-distinctive pores and cavities. However, the activated sample, Fig. 2(b) and 2(c) for 500x and 1000x magnifications respectively have rough surfaces with irregular pores, facilitating the easy diffusion of more phenol molecules into the pore structure. This could be attributed to the removal of the associated volatile matter during carbonization at high temperatures. This is in agreement with the findings of Thanapalet al. [59] where an increase in the surface porosity of char products was observed after carbonization, giving rise to a large surface area with small surface voids. The interspatial pores within the matrix of the adsorbent suggest that the produced adsorbent has good sorption properties.

On the other hand, the FTIR spectra of the raw corn cob and CCAC are presented in Fig. 3(a) and 3(b) respectively. Understanding the chemical structure of the adsorbent is key to understanding the adsorption process. The wave numbers ranged from 3693.8 to 670 cm^{-1}. The FTIR spectra results were compared with known signature of identified materials in the FTIR library [60]. Some compounds such as carboxylic acids, ethers, esters, and nitro compounds were more visible to the spectroscopy only after the activation. It could be that the associated volatile matters that were eliminated by the carbonization process previously overwhelmed these compounds. The absorption band in the 3600 cm^{-1} region is due to O-H stretching of the carboxylic acid group; while in the region of 3200 to 3300 $cm^{-1}$is due

to O-H bending of the alkanol groups. The alkanes and alkyls were in the region of 2900 – 3000 cm^{-1} due to C – H stretching while esters correspond to C – O – C stretching in the wavelength of 2200 to 2210 cm^{-1}. The nitro compounds which were not visible in the raw sample correspond to C – N stretching in the region of 1000 to 1020 cm^{-1}. N-H bending of amides group in the region of 1050-1035 cm^{-1} is due to the C-O stretching of alcohols group. The –C=C- stretch indicates the presence of alkenes while the C-Cl stretch and vibration suggest the presence of alkyl halides. The FTIR analysis revealed that the corn cob can be a good source of some hydrocarbons such as alkenes, alkyl halides, alcohols, etc. The details of the FTIR Spectroscopy analyses of the raw and activated samples are presented in Tables 6 and 7 respectively.

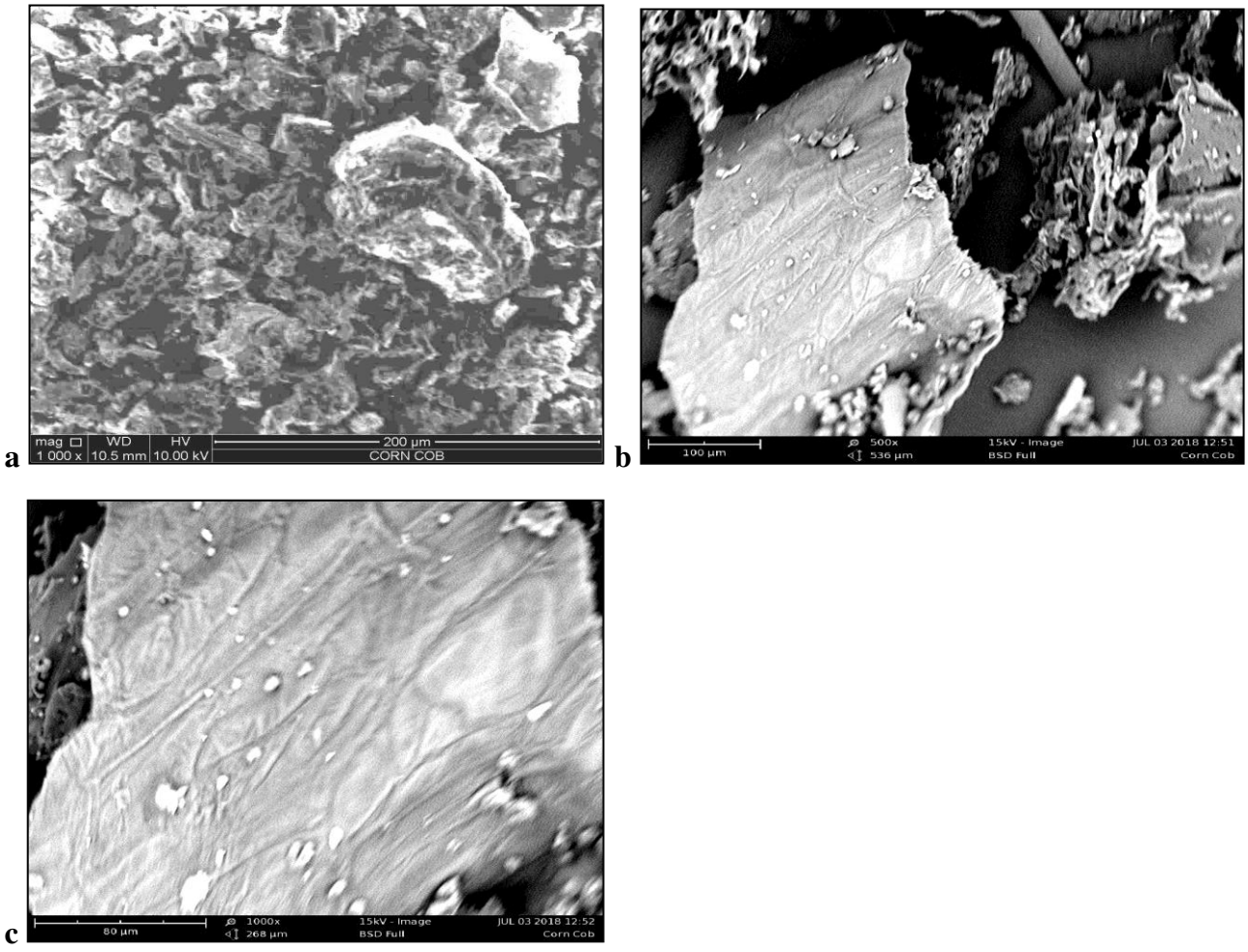

Fig. 2 SEM images of (**a**) raw corn at 500x, (**b**) CCAC at 500x, (**c**) CCAC at 1000x.

312

313

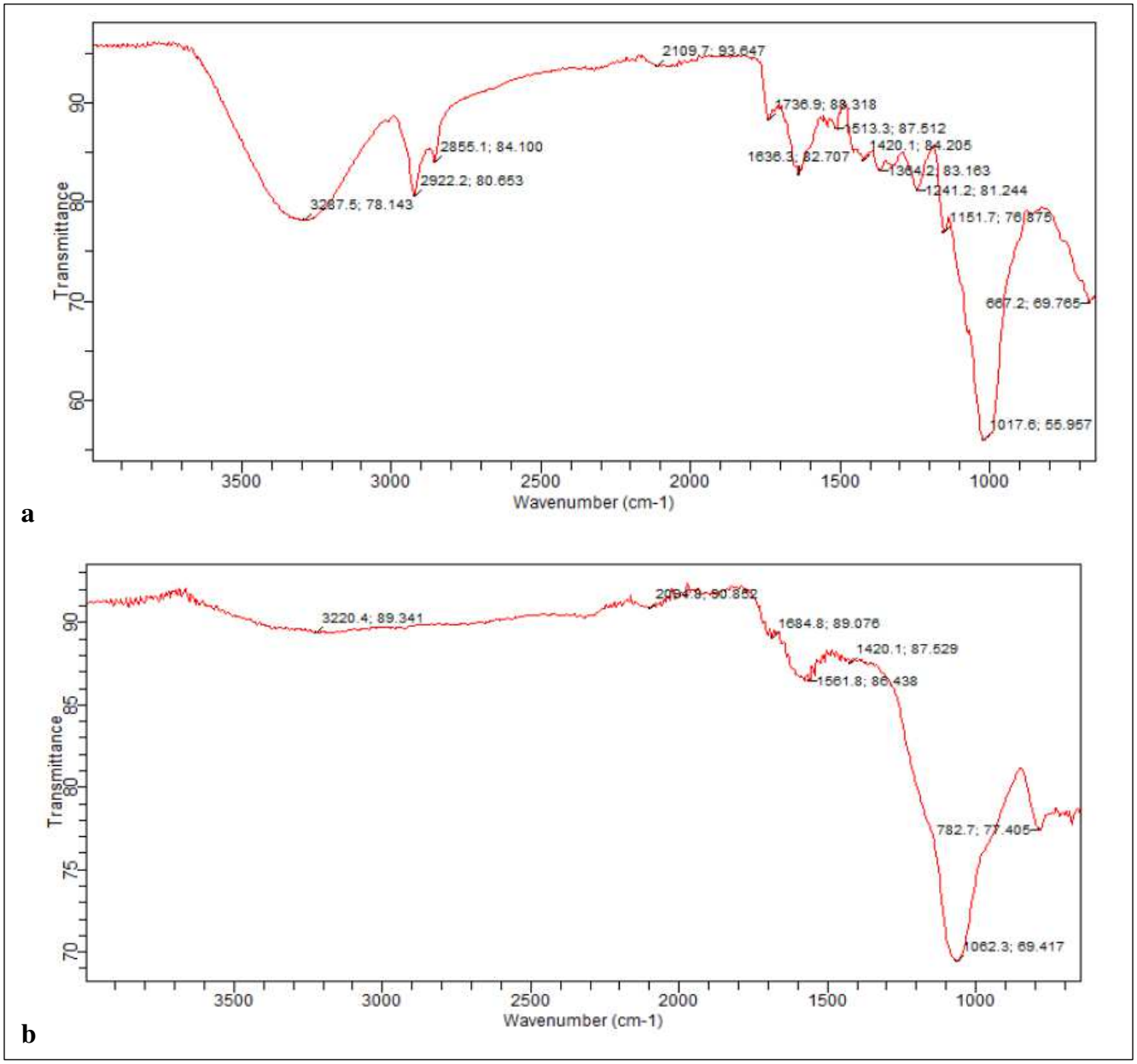

Fig. 3 FTIR spectrum of (**a**) raw corn cob; (**b**) CCAC

3.2 Effects of operating parameters

3.2.1 Effect of flow rate

The effect of flow rates on the breakthrough curves is presented in Fig. 4. This was determined by operating the column adsorption process at flow rates of 9ml/min, 13ml/min, and 18ml/min while keeping other parameters constant at 10cm bed height, 100mg/l inlet phenol concentration, 300µm particle size, and a maximum time of 24 hours. It could be observed that an increase in flow rate from 9ml/min to 18ml/min gave rise to steeper breakthrough curves, and reduced breakthrough and saturation times. The influence of the velocity variation along the packed adsorbent was of little significance because the residence time of the solute in the column is insufficient to reach adsorption equilibrium at a high flow rate [35]. Hence, at a high flow rate, the phenol solution exits the column before equilibrium is reached. The adsorbent had more time to contact with the adsorbate at lower flow rates, this significantly improves the mass transfer and inter-particle diffusion. This equally results in a decrease in the removal efficiency and adsorption capacity of the adsorbent as shown in Table 6. Chittoo and Sutherland [52], Nwabanneet al. [61], and Sarkar and Das [45] equally reported a similar observation in the recovery of phosphate using lime-iron sludge, removal of Pb(II) ions using oil palm empty fruit bunch, and the removal of Cr(VI) using coconut shell respectively. However, as a result of increased velocity, the MTZ increased as the flow rate increased (Table 6).

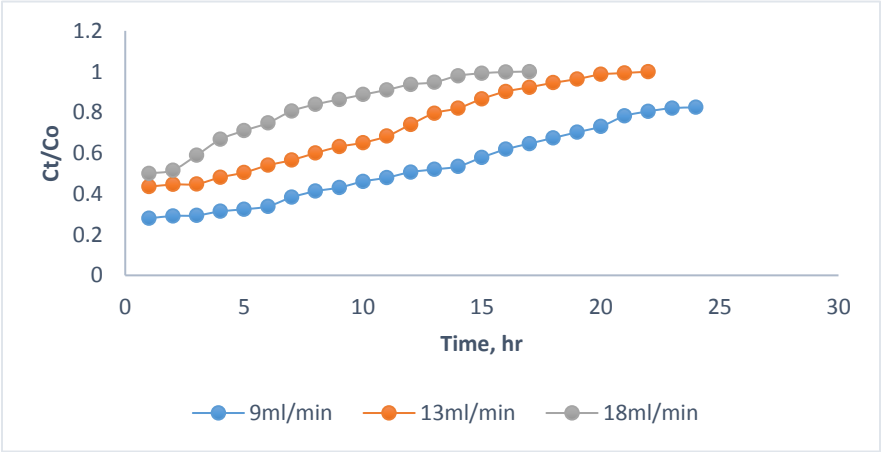

Fig. 4 Effect of flowrate on the breakthrough curve

3.2.2 Effect of inlet phenol concentration on breakthrough curve

The effect of inlet phenol concentration on the breakthrough curve is presented in Fig. 5. This investigation was carried out at 100mg/l, 200 mg/l, and 300mg/l simulated phenol concentrations. Other parameters were kept constant at 10cm bed height, 9ml/min flow rate, and particle size of 300µm. An increase in inlet phenol concentration from 100mg/l to 300mg/l resulted in a decrease in the breakthrough and saturation times. The reason could be that at lower inlet phenol concentration more time is taken to achieve a breakthrough. As the concentration of phenol molecules in the solution increased, a breakthrough was achieved faster. Other parameters that decreased with an increase in the inlet phenol concentration as presented in Table 6 include adsorption capacity at breakthrough and saturation points, removal efficiency, and volume of effluent treated at saturation. At lower inlet phenol concentration, the inflow adsorbate molecules do not overwhelm the active sites on the surface of the sorbent. Whereas, at high inlet phenol concentration, the active surfaces available for sorption are saturated earlier, leading to a reduction in adsorption capacity. As the sorbent mass and the volumetric flow rates of the solution are constant a reduction in the volume of effluent treated at saturation was observed as the sorbent molecules increased. More adsorbents will be required to remove phenol from a more concentrated feed solution. A similar trend was equally reported by Sarkar and Das [45], Chatterjee and Schiewer [50], and Madanet al. [49] in similar studies.

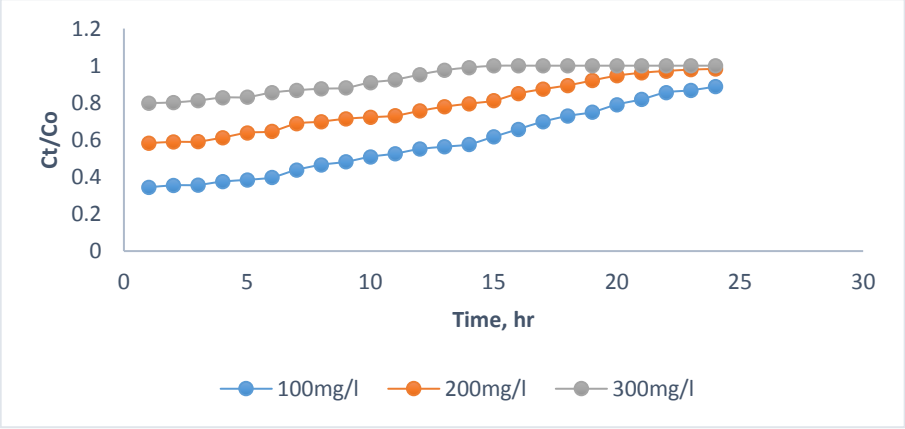

Fig. 5 Effect of influent concentration on the breakthrough curve

3.3.3 Effect of bed height on breakthrough curve

Fig. 6 presents the result of the effect of bed height on the breakthrough curves. This was studied at 5cm, 7.5cm and 10cm bed heights and at constant inlet phenol concentration, flow rate, and particle size of 100mg/l, 9ml/min, and 300µm respectively.

In the course of the experiment, it was observed that an increase in bed height resulted in a higher outlet flow resistance, this is as a result of more compact packing, the longer bed having more amount of adsorbent. This observation was equally reported by Madanet al. [49]. It could be further deduced from the result of this investigation that the breakthrough time increased with an increase in bed height. More time is required to achieve a breakthrough at higher bed height, this is because at higher bed height the phenolic ions have more available active sites for sorption. Larger bed height depicts a higher amount of adsorbent for contact with the adsorbate and this scenario results in higher phenol removal. Also, more time is required for the saturation of the bed for higher bed heights. Consequently, breakthrough and saturation points adsorption capacities, removal efficiency at saturation, the volume of effluent treated at saturation, and MTZ increased with an increase in bed height as shown in Table 6. These findings are in agreement with the results reported by Sarkar and Das [45] and Madanet al. [49] in similar studies.

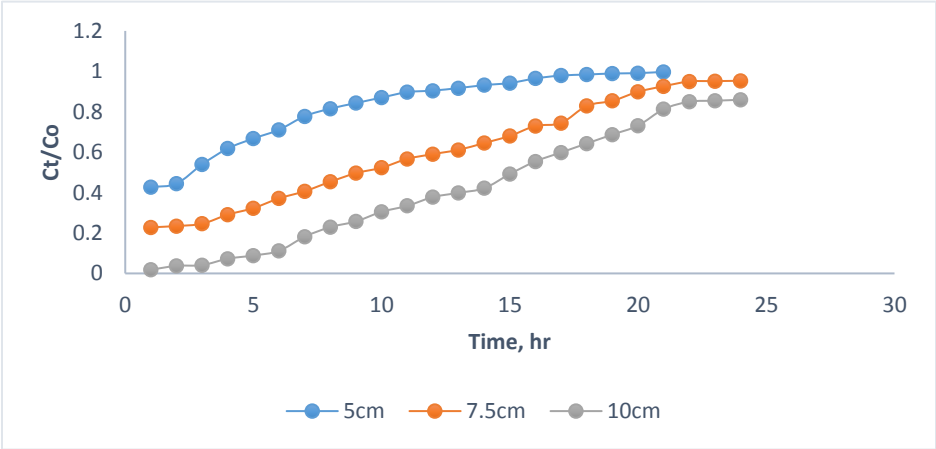

Fig. 6 Effect of bed height on the breakthrough curve

3.2.4 Effect of particle size on breakthrough curve

The effect of particle size was studied at particle sizes of 300 µm, 600 µm and 800 µm and at constant bed height, inlet phenol concentration, and flow rate of 10cm, 100mg/l, and 9ml/min respectively and presented in Fig. 7. The time taken to achieve breakthroughs and saturation decreased with an increase in particle size. This is because at increased particle size there is a less active site for sorption as a result of the reduced surface area of the adsorbent.

Smaller particle size depicts an enhanced surface area available for the interaction of the adsorbate and the adsorbent. Consequently, this results in increased breakthrough and saturation adsorption capacities, removal efficiency, and volume of effluent treated at saturation. However, the MTZ increased with the increase in particle size because as a result of the lower adsorption capacity at higher particle size, more space will be required to achieve high mass transfer. The adsorption parameters are presented in Table 6. The results of the experimental adsorption capacities have been compared with the results reported by other authors in similar studies and presented in Table 7.

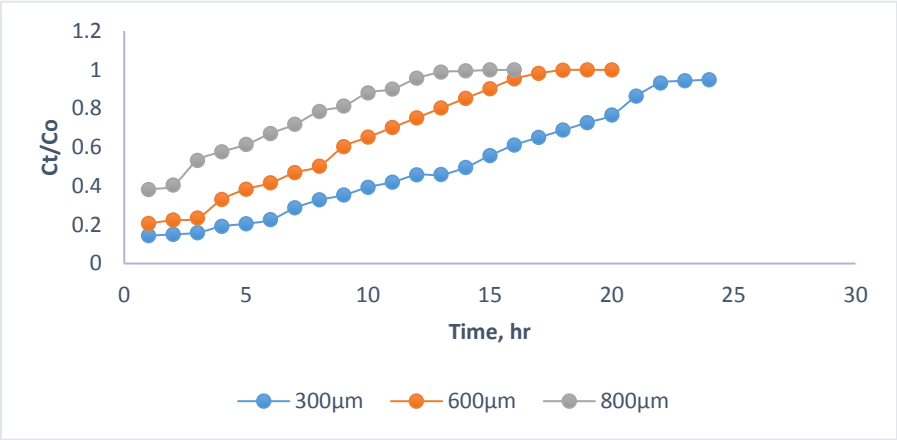

Fig. 7 Effect of particle size on the breakthrough curve

Table 6 Dynamic adsorption parameters

Process Condition	Variable	q_b (mg/g)	q_s (mg/g)	$m_{in,s}$ (mg)	$m_{out,s}$ (mg)	$m_{ads,s}$ (mg)	$Y_s(\%)$	$V_{eff,s}$ (L)	MTZ (cm)
Flow rate, Q (mL/min):	9	2.143	8.570	1296	438.955	857.045	66.13	12.96	7.50
At C_o =100mg/L, Z=10cm,	13	1.932	8.113	1638	826.698	811.301	49.53	16.38	7.62
Particle size = 300µm.	18	1.332	7.104	1728	1017.619	710.381	41.11	17.28	8.13
Inlet phenol conc. C_o (mg/L):	100	2.143	8.570	1296	438.96	857.04	66.13	12.96	7.50
At Q = 9mL/min, Z=10cm,	200	1.955	8.210	2268	1446.98	821.02	36.20	11.34	7.62
Particle size = 300µm.	300	1.115	4.740	2754	2280.04	473.96	17.21	9.18	7.65
Bed height, Z (cm):	5	1.490	4.471	486	262.44	223.56	46.00	4.86	3.33
At Q = 9mL/min, C_o =100mg/L,	7.5	1.810	8.145	972	361.10	610.90	62.85	9.72	5.83
Particle size = 300µm.	10	2.143	8.570	1296	438.95	857.04	66.13	12.96	7.50
Particle size (µm):	300	2.143	8.570	1296	438.955	857.04	66.13	12.96	7.50
At Q = 9mL/min, C_o =100mg/L,	600	1.665	5.992	972	372.762	599.24	61.65	9.72	7.22
Z = 10cm.	800	0.643	4.181	702	283.889	418.11	59.56	7.02	8.46

Table 7 Comparison of maximum adsorption capacity obtained in this work with the results of other researchers

Adsorbent	Pollutant removed	q_b (mg/g)	q_s (mg/g)	Source
Corn cob	Phenol	2.143	8.570	Present work
Silica aerogels	Phenol	NR	6.600	[62]
Pinus pinaster bark	Phenol	0.377	NR	[10]
Mowital (B30H) resin immobilized dried activated sludge	Phenol	NR	9.000	[63]
Sugarcane bagasse	Phenol	5.060	12.340	[64]

NR = Not Reported

3.3. Column kinetics study

The experimental data were fitted to Thomas, Adam-Bohart, Wolborska, and Yoon Nelson column kinetic models and analyzed via linear and nonlinear regression tools. The results of the linear and nonlinear regression analysis are presented in Tables 8 and 9 respectively.

3.3.1Thomas Model

The Thomas model is a theoretical model commonly applied in column adsorption data analysis. It is founded on the assumptions of the Langmuir isotherm model and second-order kinetic model of the batch adsorption process [65]. With the aid of the Thomas model, the maximum adsorption capacity and adsorption rate constant can be predicted for dynamic column adsorption studies. The linear and nonlinear mathematical expressions of the Thomas model are represented by Eqs. (9) and (13) respectively, where, q_e (mg/g) is the maximum or equilibrium adsorption capacity and k_{TH} (L/mg/min) is the adsorption rate constant. The amount of adsorbent in the column at a given bed height is represented by m (g). Q is the volumetric flow rate, and Ct/Co is the effluent to the inlet concentration ratio of phenol.

In the linear regression analysis, the values of q_e and k_{TH} were obtained from the linear plots of $\ln\left(\frac{C_t}{C_o} - 1\right)$ against time shown in Fig. 8. The results are presented in Table 8 for various values of volumetric flow rate, inlet phenol concentration, bed height, and particle size. It could be deduced from the results that as the flow rate and particle size increased from 9ml/min to 18ml/min and from 300µm to 800µm respectively the q_e values decreased while the k_{TH} increased. The decrease of adsorption capacity with an increase in flow rate is because the solute does not have sufficient residence time in the column to achieve equilibrium at a high flow rate, whereas the adsorbent would have more time to contact with the adsorbate at a low flow rate. Similarly, smaller particle size depicts enhanced surface area available for the interaction of the adsorbate and the adsorbent, this accounts for while adsorption capacity decreased with an increase in particle size. Both q_e and k_{TH} decreased with an increase in initial phenol concentration. This is because, at high inlet phenol concentration, the active surfaces available for sorption are saturated earlier, leading to a reduction in adsorption capacity. As regards the bed height, q_e increased with an increase in bed height, this is because at higher bed height the phenolic ions have more available active sites for sorption, thereby leading to an increase in the adsorption capacity. The trend of the relationship between the adsorption capacity and the process

variables obtained in this study is similar to the trend reported by Shanmugamet al. [58] in a similar study. The high correlation coefficient values ($R^2 > 0.9$) obtained in the analysis in most cases showed that the Thomas model fitted the experimental data quite well. A maximum adsorption capacity of 8.026 (mg/g) was predicted by the model at bed height 10cm, initial phenol concentration, 100mg/l, flow rate, 9ml/min, and particle size 300µm.

The nonlinear regression analysis of the Thomas model was carried out with the aid of Microsoft Excel's Solver Extension software program. The model parameters obtained at different process variables are presented in Table 9. The q_e values were found to decrease with an increase in volumetric flow rate, influent phenol concentration, and particle size, while it increased with an increase in bed height. K_{TH} increased with an increase in flow rate, bed height and particle size but showed no linear relation with the initial phenol concentration. The correlation coefficients obtained in the nonlinear analysis were higher than those obtained via the linear tool. R^2 values of up to 1.0000 were obtained in most cases. Various error functions viz. RMSE, χ^2, SSE, SAE, and ARE were further used to assess the error distribution between the experimental data and the model predicted data. In most cases, the values of the error functions were far less than zero indicating a minimal error in the prediction of the model parameters. A maximum adsorption capacity of 8.685 (mg/g) was predicted at the same experimental conditions as with the linear analysis.

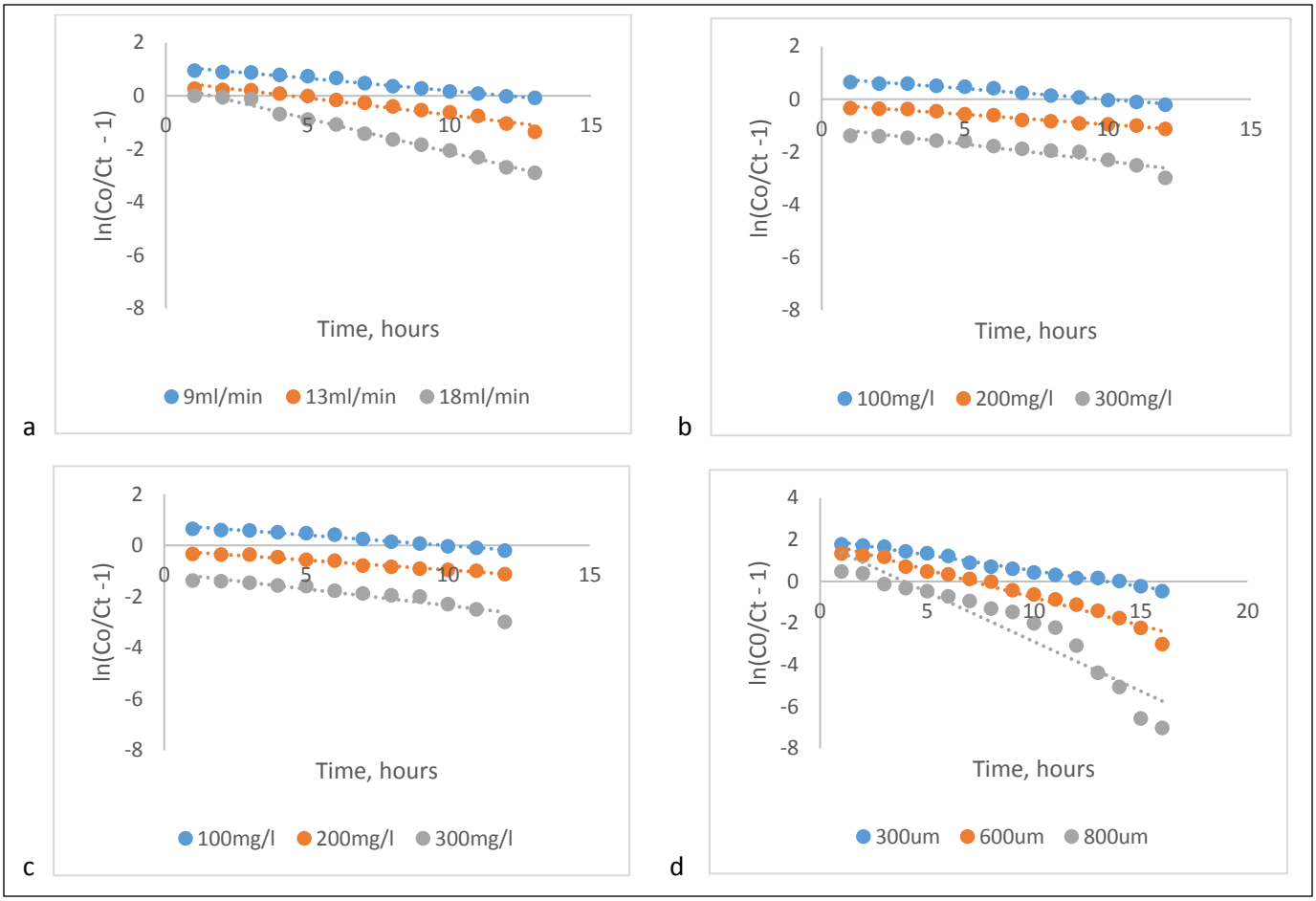

Fig. 8 Linear plots of Thomas kinetic model: **(a)** at different flow rates; **(b)** at different influent concentration (**c**) at different bed heights; (**d**) at different particle sizes

3.3.2 Adam-Bohart Model

Adams-Bohart model is based on the assumption that the adsorption capacity is directly proportional to the residual capacity as well as the initial pollutant concentration [65]. The linear and nonlinear forms of the model are represented by Eqs. (10) and (14) respectively, where, k_{AB} is the kinetic constant (L/mg min), N_o is the saturation concentration (mg/L), Z is the bed height (cm), while U_o depicts the linear velocity (cm/min).

In the linear regression analysis, the values of N_o and k_{AB} were calculated from the linear plots of $\ln\frac{C_t}{C_o}$ against time as shown in Fig. 9. The results are presented in Table 8. The results showed that N_o values increased with flow rate and influent phenol concentration but decreased with an increase in bed height and particle size. On the other hand, k_{AB} decreased with an increase in flow rate and influent phenol concentration but increased with an increase in bed height. The values of N_o were in the range of 769.845 and 2985.340 (mg/L), while k_{AB} ranged from 0.000057 to

0.00233 (L/mg min). The range of values obtained in this study for N_o and k_{AB} and how the values relate with the process variables are similar to the results reported by Ajmaniet al. [65] for the removal hexavalent chromium using activated carbon synthesized from Phanera vahlii fruit biomass. The experimental values were well fitted to the Adams-Bohart model as the R^2 values were above 0.90 in most cases.

The result of the nonlinear regression analysis is presented in Table 9. As was the case with the linear analysis, the N_o values increased with flow rate and influent phenol concentration but decreased with an increase in bed height and particle size. Similarly, k_{AB} decreased with an increase in flow rate, influent phenol concentration, and particle size but increased with an increase in bed height. The correlation coefficients obtained were quite high, up to 1.0000 in most cases. The values of other error functions such as RMSE, χ^2, SSE, SAE, and ARE were also very low, up to three decimal places lower than zero in some cases. This shows that nonlinear analysis is a better approach for fitting the experimental values to the Adams-Bohart model.

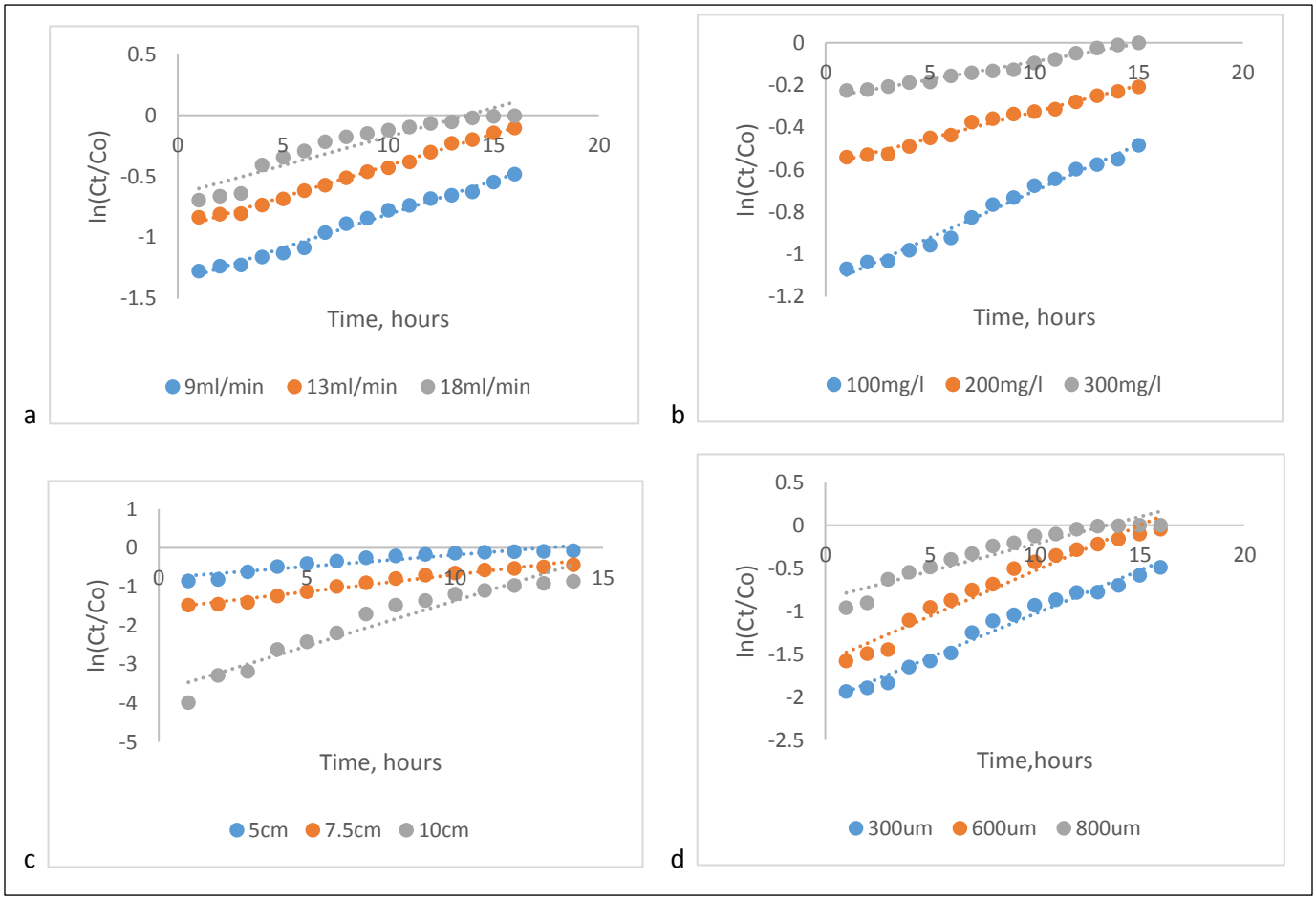

Fig. 9 Linear plots of Adam-Bohart kinetic model: (**a**) at different flow rates; (**b**) at different influent concentration; (**c**) at different bed heights; (**d**) at different particle size

3.3.3 Wolborska Model

The Wolborska model generally describes the concentration distribution in the packed bed for the low concentration region of the breakthrough curve [66]. The mathematical expressions for the linear and nonlinear forms of the model are represented by Eqs. (11) and (15) respectively. The parameters are similar to that of the Adams-Bohart model, where N_o (mg/L) represents the saturation concentration, β (L/min), the kinetic coefficient of external mass transfer, Z is the bed height (cm), while U_o depicts the linear velocity (cm/min).

The values of N_o and β were calculated from the linear plots of $\ln\frac{C_t}{C_o}$ against time in the linear regression analysis as shown in Fig. 10 and presented in Table 8. The N_o values obtained in the Wolborska model are the same as in the Adams-Bohart model this could be as a result of the similarity in the mathematical expressions of both models. N_o increased with an increase in flow rate and influent phenol concentration but decreased with an increase in bed height and particle size. This depicts the similarities existing between the two models. Similarly, β decreased with an increase in flow rate and influent phenol concentration but increased with an increase in bed height. The β values are in the range of 0.1486 to 2.1186 (L/min). Shanmugamet al. [58] reported a similar trend and equally affirmed that β is an effective coefficient reflecting on the effects of both mass transfer in the liquid phase and axial diffusion. The R^2 values were higher than 0.88 in all cases, depicting a good correlation with the experimental data.

The model parameters obtained via the nonlinear approach are presented in Table 9. The result showed that both the N_o and β values obtained via the nonlinear approach related to the process variables in the same manner as was with the linear analysis. However, while a maximum N_o value of 2985.34 mg/L, was recorded for the linear approach, 2687.956 mg/L, was obtained in the nonlinear approach. Similarly, β values for the linear approach were in the range of 0.1486 to 2.1186 (L/min) while the nonlinear result ranged from 0.1562 to 2.0435 (L/min). Very high correlation coefficients, up to 1.0000 in most cases were obtained. The values of other error functions such as RMSE, χ^2, SSE, SAE, and ARE were also very low, less than zero in most cases, depicting minimal error in the prediction of the model parameters

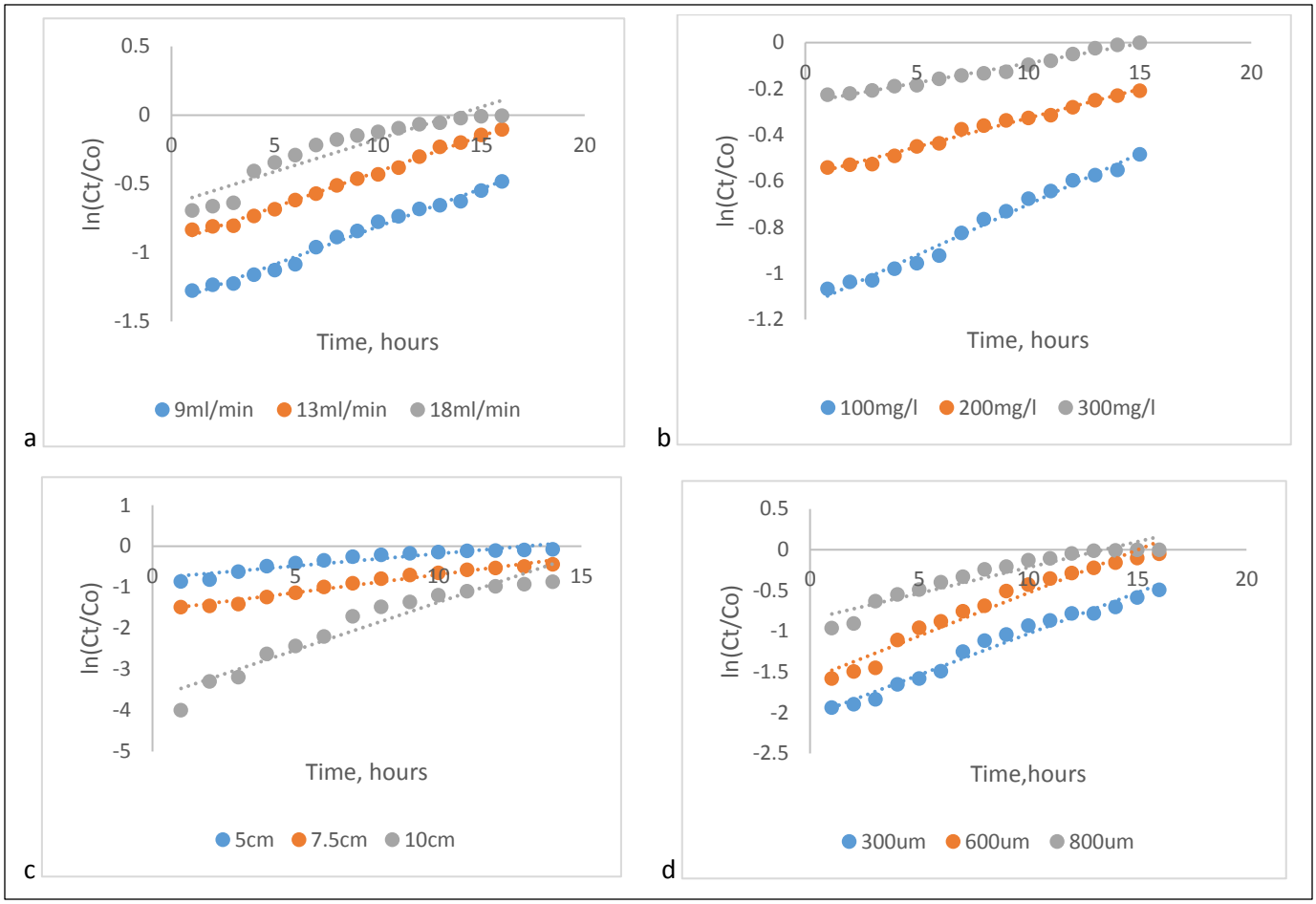

Fig. 10 Linear plots of Wolborska kinetic model: **(a)** at different flow rates; (**b**) at different influent concentration; **(c)** at different bed heights; **(d)** at different particle size

3.3.4 Yoon Nelson Model

The model proposed by Yoon-Nelson considers that the probability of adsorption of each molecule is directly proportional to the probability of adsorbate breakthrough on the adsorbent and the probability of adsorbate adsorption [65]. The linear and nonlinear mathematical forms of the model are expressed as Eqs. (12) and (16) respectively. The key parameters of the model are k_{YN} and τ, where, k_{YN} is the Yoon-Nelson rate constant (L/min) and τ represents the time required for 50 % adsorbate breakthrough.

The linear regression analysis was accomplished by plotting $\ln\left(\frac{C_t}{C_o - C_t}\right)$ against time as shown in Fig. 11. The values of the k_{YN} and τ obtained are presented in Table 8. It could be observed that the values of τ decreased with an increase

in flow rate, influent phenol concentration, and particle size but increased with an increase in bed height. The increase of τ with bed height is because higher bed height depicts a greater number of adsorption sites, requiring more time to achieve a 50 % adsorbate breakthrough. The decrease in τ with influent phenol concentration is because less time would be required to achieve a 50 % breakthrough since more phenol is readily available for the available active sites. Similarly, the decrease of τ values observed as the flow rate increased is because a higher flow rate depicts higher flow velocity a condition that means that the phenol ions are supplied to the available active sites faster than it would be at lower flow rates. On the other hand, the Yoon-Nelson, k_{YN} increased with an increase in flow rate, influent phenol concentration, and particle size but showed no linear relation with bed height. Ajmaniet al. [65] reported a similar result in a similar study. The R^2 values are high in most cases up to 0.98 and as low as 0.67 at 300mg/l influent phenol concentration.

The results obtained from the nonlinear regression analysis are presented in Table 9. It could be deduced from the results that both the τ and k_{YN} values obtained via the nonlinear approach related to the process variables in the same manner as was with the linear analysis. The R^2 values obtained in the nonlinear approach were far higher than those obtained in the linear approach, reaching up to 1.0000 in some cases and greater than 0.9900 in most cases. The error functions were also low, less than zero in some cases, and greater than zero in some other cases. The Yoon-Nelson model fits the experimental data well but not the best in comparison with other Thomas, Adams-Boha, and Wolborska models when the R^2 values and error functions are considered.

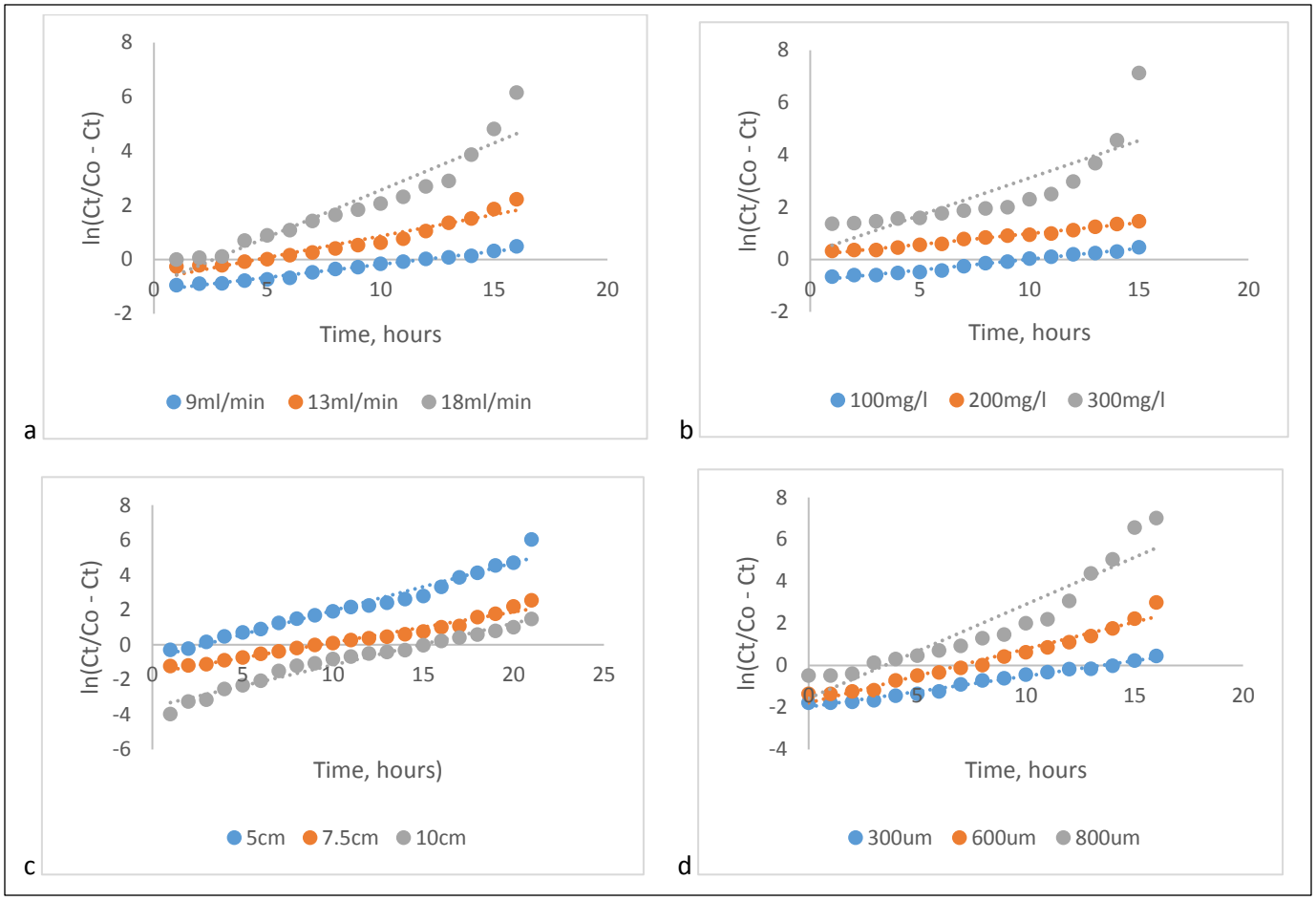

Fig. 11 Linear plots of Yoon-Nelson kinetic model: **(a)** at different flow rates; **(b)** at different influent concentrations; **(c)** at different bed heights; **(d)** at different particle sizes

[Insert Table 8 here]

[Insert Table 9 here]

3.4 Comparison of the maximum adsorption capacities obtained experimentally with the values predicted via linear and nonlinear regression analysis.

The values of the adsorption capacities obtained experimentally and the values predicted via the linear and nonlinear regression analysis of the Thomas model were presented in Table 10 for direct comparison. It could be deduced from Table 10 that the adsorption capacities predicted by the nonlinear regression analysis are higher in proximity to the experimental values when compared to the values predicted by the linear regression approach. A maximum q_e value

of 8.570 mg/g was obtained experimentally, 8.685 mg/g was obtained from nonlinear regression analysis, while linear regression analysis gave a value of 8.026 mg/g at the same experimental condition. It can also be seen in Table 10 that the values of the correlation coefficient (R^2) depicting the goodness of fit of the experimental data to the model are higher for nonlinear regression analysis, up to 1.0000 in most cases. This shows that the nonlinear regression approach should be followed for more accurate predictions of the adsorption parameters.

Table 10 Comparison of the linear and nonlinear maximum adsorption capacities with the experimental values

Process Condition	**Variable**	**Adsorption capacity at equilibrium, q_e, (mg/g)**				
		Linear		**Nonlinear**		**Experimental**
		q_e	**R^2**	**q_e**	**R^2**	**q_e**
Flow rate, Q (mL/min):	9	**6.509**	0.9800	**8.659**	1.0000	**8.570**
At C_o =100mg/L, Z=10cm, Particle	13	**3.391**	0.9540	**4.623**	0.9924	**8.113**
size = 300µm.	18	**1.710**	0.9900	**3.404**	1.0000	**7.104**
Inlet phenol conc. C_o (mg/L):	100	**5.357**	0.9720	**8.207**	1.0000	**8.570**
At Q = 9mL/min, Z=10cm,	200	**2.746**	0.9770	**5.060**	1.0000	**8.210**
Particle size = 300µm.	300	**2.039**	0.8940	**3.526**	1.0000	**4.740**
Bed height, Z (cm):	5	**3.065**	0.9650	**4.165**	1.0000	**4.471**
At Q = 9mL/min, C_o =100mg/L,	7.5	**6.664**	0.9710	**7.042**	0.9861	**8.145**
Particle size = 300µm.	10	**8.026**	0.9700	**8.685**	0.9907	**8.570**
Particle size (µm):	300	**7.232**	0.9880	**8.647**	1.0000	**8.570**
At Q = 9mL/min, C_o =100mg/L,	600	**3.832**	0.9700	**4.013**	0.9998	**5.992**
Z = 10cm.	800	**2.119**	0.8910	**1.881**	1.0000	**4.181**

4. Conclusion

This work investigated the effectiveness of activated carbon synthesized from locally and abundantly available corn cob for the removal of phenol from aqueous solution in a packed bed dynamic mode. The experiments showed that the adsorption process depends on flow rate, initial phenol concentration, bed height, and particle size. The adsorption

capacity was found to be favored by lower flow rate, initial phenol concentration, and particle size as well as the higher bed height. Similarly, breakthrough time increased with an increase in bed height but decreased with an increase in flow rate, initial phenol concentration, and particle size. Various parameters needed for the successful design of a dynamic adsorption column viz. adsorption capacities at breakthrough and saturation points, the volume of effluent treated at saturation point, length of mass transfer zone (MTZ), and percentage phenol removal were estimated experimentally. At optimum condition, the adsorption capacities at breakthrough and saturation points were 2.143 and 8.570 mg/g respectively, the volume of effluent treated at saturation point was 12.96L, the length of mass transfer zone (MTZ) was 7.50cm and 66.13% phenol removal was achieved. The experimental data were subjected to Thomas, Adam Bohart, Wolborska, and Yoon Nelson's dynamic adsorption models and analyzed via linear and nonlinear regression tools. The four models fitted the experimental data quite well but Thomas, Adam Bohart, and Wolborska models gave a better fit in comparison with the Yoon Nelson model. Overall, the nonlinear regression analysis approach is recommended for the analysis of dynamic adsorption models because the predicted parameters obtained via the nonlinear tool were closer to the experimental data than those obtained via linear regression analysis. The correlation coefficients of the nonlinear regression analysis were in most cases up to 1.0000. This study has shown that CCAC is effective for the decontamination of phenol contaminated aqueous effluents. The study also provided experimentally generated data needed for the design of a packed bed adsorption column for wastewater decontamination.

Nomenclature

$\mathbf{C_o}$ = initial phenol concentration (mg/L)

$\mathbf{C_t}$ = phenol concentration at time t (mg/L)

$\boldsymbol{q_b}$ = Adsorption capacity at breakthrough (mg/g)

$\boldsymbol{q_s}$ = Adsorption capacity at saturation (mg/g)

Z = bed height (cm)

$\boldsymbol{Q}$ = flow rate of the influent (ml/min)

$\boldsymbol{m}$ = mass of adsorbent in column (g)

t = service time or time (min)

MTZ = Length of Mass Transfer Zone (cm)

669 $V_{eff,s}$ = Volume of effluent treatment at saturation (L)

670 U_o = linear velocity of effluent (cm/min)

671 K_{AB} = Adam-Bohart kinetic constant (L/mg.min)

672 **No** = Saturation concentration (mg/L)

673 K_{YN} = Yoon-Nelson rate constant (L/min)

674 τ = time required for 50 % adsorbate breakthrough (h)

675 K_{TH} = Thomas kinetic rate constant (L/mg.min)

676 q_{TH} = Adsorption capacity predicted by Thomas model (mg/g)

677 β = Wolborska kinetic coefficient of external mass transfer (L/min)

678

679 **Declarations**

680 - **Funding:** No funds, grants, or other support was received.

681 - **Conflicts of interest:** The authors have no conflicts of interest to declare that are relevant to the content of
682 this article.

683 - **Availability of data and material:** All data generated or analyzed during this study are included in this
684 article.

685 - **Code availability:** Not applicable

686 - **Authors' Contributions:** All authors contributed to the study conception and design. Material preparation,
687 data collection and analysis were performed by Ositadinma Chamberlain Iheanacho, Joseph Tagbo
688 Nwabanne and Chijioke Elijah Onu. The first draft of the manuscript was written by Christopher Chiedozie
689 Obi and all authors commented on previous versions of the manuscript. All authors read and approved the
690 final manuscript.

691

692 **References**

693 1. Mahugo-Santana C, Sosa-Ferrera Z, Torres-Padrón ME, Santana-Rodríguez JJ. Analytical methodologies for
694 the determination of nitroimidazole residues in biological and environmental liquid samples: A review.
695 Analytica Chimica Acta. 2010;665:113-122.DOI: 10.1016/j.aca.2010.03.022.
696 2. Hamad HT. Removal of phenol and inorganic metals from wastewater using activated ceramic. Journal of
697 King Saud University - Engineering Sciences. 2020.DOI: 10.1016/j.jksues.2020.04.006.

3. Abbas MN, Al-Madhhachi A-ST, Esmael SA. Quantifying soil erodibility parameters due to wastewater chemicals. International Journal of Hydrology Science and Technology. 2019;9:550-568.
4. Krishnaiah D, Bono A, Sarbatly R, Anisuzzaman SM. Antioxidant activity and total phenolic content of an isolated Morinda citrifolia L. methanolic extract from Poly-ethersulphone (PES) membrane separator. Journal of King Saud University - Engineering Sciences. 2015;27:63-67.DOI: 10.1016/j.jksues.2013.01.002.
5. Anisuzzaman S, Bono A, Krishnaiah D, Tan YZ. A study on dynamic simulation of phenol adsorption in activated carbon packed bed column. Journal of King Saud university-engineering sciences. 2016;28:47-55.
6. Malakootian M, Jafari Mansoorian H, Alizadeh M, Baghbanian A. Phenol Removal from Aqueous Solution by Adsorption Process: Study of The Nanoparticles Performance Prepared from Alo vera and Mesquite (Prosopis) Leaves. Scientia Iranica. 2017;24:3041-3052.
7. Abid MF, Abdulla ON, Kadhim AF. Study on removal of phenol from synthetic wastewater using solar photo catalytic reactor. Journal of King Saud University - Engineering Sciences. 2019;31:131-139.DOI: 10.1016/j.jksues.2017.03.002.
8. Mahmoud MA. Kinetics studies of uranium sorption by powdered corn cob in batch and fixed bed system. Journal of Advanced Research. 2016;7:79-87.DOI: 10.1016/j.jare.2015.02.004.
9. Patel H. Fixed-bed column adsorption study: a comprehensive review. Applied Water Science. 2019;9.DOI: 10.1007/s13201-019-0927-7.
10. Vazquez G, Alonso R, Freire S, Gonzalezalvarez J, Antorrena G. Uptake of phenol from aqueous solutions by adsorption in a Pinus pinaster bark packed bed. Journal of Hazardous Materials. 2006;133:61-67.DOI: 10.1016/j.jhazmat.2004.12.041.
11. Malkoc E, Nuhoglu Y, Abali Y. Cr (VI) adsorption by waste acorn of Quercus ithaburensis in fixed beds: Prediction of breakthrough curves. Chemical Engineering Journal. 2006;119:61-68.
12. Masoud MS, El-Saraf WM, Abdel-Halim AM, Ali AE, Mohamed EA, Hasan HM. Rice husk and activated carbon for waste water treatment of El-Mex Bay, Alexandria Coast, Egypt. Arabian Journal of Chemistry. 2016;9:S1590-S1596.
13. Alalwan HA, Abbas MN, Abudi ZN, Alminshid AH. Adsorption of thallium ion (Tl+ 3) from aqueous solutions by rice husk in a fixed-bed column: Experiment and prediction of breakthrough curves. Environmental Technology & Innovation. 2018;12:1-13.
14. Zhang K, Khan A, Sun P, Zhang Y, Taraqqi-A-Kamal A, Zhang Y. Simultaneous reduction of Cr (VI) and oxidization of organic pollutants by rice husk derived biochar and the interactive influences of coexisting Cr (VI). Science of The Total Environment. 2020;706:135763.
15. Kong S, Jin B, Quan X, Zhang G, Guo X, Zhu Q, et al. MnO2 nanosheets decorated porous active carbon derived from wheat bran for high-performance asymmetric supercapacitor. Journal of Electroanalytical Chemistry. 2019;850:113412.DOI: https://doi.org/10.1016/j.jelechem.2019.113412.
16. Das S, Singh S, Garg S. Evaluation of wheat bran as a biosorbent for potential mitigation of dye pollution in industrial waste waters. Oriental Journal of Chemistry. 2019;35:1565-1573.
17. Alalwan HA, Kadhom MA, Alminshid AH. Removal of heavy metals from wastewater using agricultural byproducts. Journal of Water Supply: Research and Technology—AQUA. 2020;69:99-112.
18. Purnomo CW, Salim C, Hinode H. Preparation and characterization of activated carbon from bagasse fly ash. Journal of Analytical and Applied Pyrolysis. 2011;91:257-262.
19. Aslam Z, Shawabkeh RA, Hussein IA, Al-Baghli N, Eic M. Synthesis of activated carbon from oil fly ash for removal of H2S from gas stream. Applied Surface Science. 2015;327:107-115.
20. Muriithi GN, Petrik LF, Doucet FJ. Synthesis, characterisation and CO2 adsorption potential of NaA and NaX zeolites and hydrotalcite obtained from the same coal fly ash. Journal of CO2 Utilization. 2020;36:220-230.
21. Subramaniam R ,Ponnusamy SK. Novel adsorbent from agricultural waste (cashew NUT shell) for methylene blue dye removal: optimization by response surface methodology. Water Resources and Industry. 2015;11:64-70.
22. Sanmuga Priya E ,Senthamil Selvan P. Water hyacinth (Eichhornia crassipes) – An efficient and economic adsorbent for textile effluent treatment – A review. Arabian Journal of Chemistry. 2017;10:S3548-S3558.DOI: https://doi.org/10.1016/j.arabjc.2014.03.002.
23. Mazlan MAF, Uemura Y, Yusup S, Elhassan F, Uddin A, Hiwada A, et al. Activated carbon from rubber wood sawdust by carbon dioxide activation. Procedia engineering. 2016;148:530-537.
24. Kumar A ,Gupta H. Activated carbon from sawdust for naphthalene removal from contaminated water. Environmental Technology & Innovation. 2020;20:101080.

25. Ahmad M, Lee SS, Dou X, Mohan D, Sung J-K, Yang JE, et al. Effects of pyrolysis temperature on soybean stover-and peanut shell-derived biochar properties and TCE adsorption in water. Bioresource technology. 2012;118:536-544.
26. Giraldo L ,Moreno-Piraján JC. Study of adsorption of phenol on activated carbons obtained from eggshells. Journal of Analytical and Applied Pyrolysis. 2014;106:41-47.DOI: https://doi.org/10.1016/j.jaap.2013.12.007.
27. Wakchaure G, Das L, Kolar P. Eggshell as an Inexpensive Adsorbent for Removal of p-Cresol. Transactions of the ASABE. 2016;59:965-974.
28. Solgi M, Najib T, Ahmadnejad S, Nasernejad B. Synthesis and characterization of novel activated carbon from Medlar seed for chromium removal: Experimental analysis and modeling with artificial neural network and support vector regression. Resource-Efficient Technologies. 2017;3:236-248.DOI: https://doi.org/10.1016/j.reffit.2017.08.003.
29. Gratuito MKB, Panyathanmaporn T, Chumnanklang R-A, Sirinuntawittaya N, Dutta A. Production of activated carbon from coconut shell: Optimization using response surface methodology. Bioresource technology. 2008;99:4887-4895.
30. Li W, Peng J, Zhang L, Yang K, Xia H, Zhang S, et al. Preparation of activated carbon from coconut shell chars in pilot-scale microwave heating equipment at 60 kW. Waste management. 2009;29:756-760.
31. Hidayu A ,Muda N. Preparation and characterization of impregnated activated carbon from palm kernel shell and coconut shell for CO2 capture. Procedia Engineering. 2016;148:106-113.
32. Rashidi NA ,Yusup S. Potential of palm kernel shell as activated carbon precursors through single stage activation technique for carbon dioxide adsorption. Journal of Cleaner Production. 2017;168:474-486.
33. Naguib DM ,Badawy NM. Phenol removal from wastewater using waste products. Journal of Environmental Chemical Engineering. 2020;8:103592.DOI: https://doi.org/10.1016/j.jece.2019.103592.
34. Achak M, Hafidi A, Mandi L, Ouazzani N. Removal of phenolic compounds from olive mill wastewater by adsorption onto wheat bran. Desalination and Water Treatment. 2014;52:2875-2885.
35. Abdelkreem M. Adsorption of Phenol from Industrial Wastewater Using Olive Mill Waste. APCBEE Procedia. 2013;5:349-357.DOI: 10.1016/j.apcbee.2013.05.060.
36. Aremu MO, Arinkoola AO, Olowonyo IA, Salam KK. Improved phenol sequestration from aqueous solution using silver nanoparticle modified Palm Kernel Shell Activated Carbon. Heliyon. 2020;6:e04492.DOI: https://doi.org/10.1016/j.heliyon.2020.e04492.
37. Mittal A, Kaur D, Malviya A, Mittal J, Gupta V. Adsorption studies on the removal of coloring agent phenol red from wastewater using waste materials as adsorbents. Journal of colloid and interface science. 2009;337:345-354.
38. Srihari V ,Das A. The kinetic and thermodynamic studies of phenol-sorption onto three agro-based carbons. Desalination. 2008;225:220-234.
39. Alam Z, Muyibi SA, Toramae J. Statistical optimization of adsorption processes for removal of 2,4-dichlorophenol by activated carbon derived from oil palm empty fruit bunches. Journal of Environmental Sciences. 2007;19:674-677.DOI: https://doi.org/10.1016/S1001-0742(07)60113-2.
40. Girei AA, Saingbe ND, Ohen SB, Umar KO. Economics of small-scale maize production in Toto local government area, Nasarawa state, Nigeria. Agrosearch. 2018;18:90.DOI: 10.4314/agrosh.v18i1.8.
41. Duan X-L, Yuan C-G, Jing T-T, Yuan X-D. Removal of elemental mercury using large surface area micro-porous corn cob activated carbon by zinc chloride activation. Fuel. 2019;239:830-840.
42. Manzoor Q, Sajid A, Hussain T, Iqbal M, Abbas M, Nisar J. Efficiency of immobilized Zea mays biomass for the adsorption of chromium from simulated media and tannery wastewater. Journal of Materials Research and Technology. 2019;8:75-86.DOI: https://doi.org/10.1016/j.jmrt.2017.05.016.
43. Nowicki P, Kazmierczak-Razna J, Skibiszewska P, Wiśniewska M, Nosal-Wiercińska A, Pietrzak R. Production of activated carbons from biodegradable waste materials as an alternative way of their utilisation. Adsorption. 2016;22:489-502.
44. Shakoor MB, Niazi NK, Bibi I, Shahid M, Saqib ZA, Nawaz MF, et al. Exploring the arsenic removal potential of various biosorbents from water. Environment international. 2019;123:567-579.
45. Sarkar S ,Das SK. Removal of hexavalent chromium from aqueous solution using natural adsorbents–column studies. Int J Eng Res Technol. 2016;5:370-377.
46. Han R, Wang Y, Zou W, Wang Y, Shi J. Comparison of linear and nonlinear analysis in estimating the Thomas model parameters for methylene blue adsorption onto natural zeolite in fixed-bed column. Journal of Hazardous Materials. 2007;145:331-335.

47. Horwitz W ,Latimer GW. Official methods of analysis of AOAC International. 2005, Gaithersburg, Md.: AOAC International.
48. Sivakumar B, Kannan C, Karthikeyan S. Preparation and characterization of activated carbon prepared from balsamodendron caudatum wood waste through various activation processes. Chem. 2012;5:321-327.
49. Madan SS, De BS, Wasewar KL. Adsorption performance of packed bed column for benzylformic acid removal using CaO2 nanoparticles. Chemical Data Collections. 2019;23:100267.
50. Chatterjee A ,Schiewer S. Biosorption of cadmium (II) ions by citrus peels in a packed bed column: effect of process parameters and comparison of different breakthrough curve models. CLEAN–Soil, Air, Water. 2011;39:874-881.
51. Can M. Studies of the kinetics for rhodium adsorption onto gallic acid derived polymer: the application of nonlinear regression analysis. system. 2015;10.
52. Chittoo BS ,Sutherland C. Column breakthrough studies for the removal and recovery of phosphate by lime-iron sludge: Modeling and optimization using artificial neural network and adaptive neuro-fuzzy inference system. Chinese Journal of Chemical Engineering. 2020;28:1847-1859.DOI: https://doi.org/10.1016/j.cjche.2020.02.022.
53. Hossain M, Ngo H, Guo W. Introductory of Microsoft Excel SOLVER function-spreadsheet method for isotherm and kinetics modelling of metals biosorption in water and wastewater. Journal of Water Sustainability. 2013.
54. Samarghandi M, Hadi M, Moayedi S, BARJESTEH AF. Two-parameter isotherms of methyl orange sorption by pinecone derived activated carbon. 2009.
55. López-Luna J, Ramírez-Montes LE, Martinez-Vargas S, Martínez AI, Mijangos-Ricardez OF, María del Carmen A, et al. Linear and nonlinear kinetic and isotherm adsorption models for arsenic removal by manganese ferrite nanoparticles. SN Applied Sciences. 2019;1:950.
56. Ayawei N, Ebelegi AN, Wankasi D. Modelling and interpretation of adsorption isotherms. Journal of Chemistry. 2017;2017.
57. Enaime G, Ennaciri K, Ounas A, Baçaoui A, Seffen M, Selmi T, et al. Preparation and characterization of activated carbons from olive wastes by physical and chemical activation: application to Indigo carmine adsorption. J. Mater. Environ. Sci. 2017;8:4125-4137.
58. Shanmugam D, Alagappan M, Rajan RK. Bench-scale packed bed sorption of Cibacron blue F3GA using lucrative algal biomass. Alexandria Engineering Journal. 2016;55:2995-3003.
59. Thanapal SS, Chen W, Annamalai K, Carlin N, Ansley RJ, Ranjan D. Carbon dioxide torrefaction of woody biomass. Energy & fuels. 2014;28:1147-1157.
60. Stuart B. Infrared spectroscopy. Kirk-Othmer encyclopedia of chemical technology. 2000.
61. Nwabanne J, Okoye A, Lebele-Alawa B. Packed bed column studies for the removal of lead (ii) using oil palm empty fruit bunch. European Journal of Scientific Research. 2011;63:296-305.
62. Marques J, Matias T, Valente AJM, Portugal A, Quina MJ, Gando-Ferreira L, et al. Adsorption of phenol on silica aerogels using a stirred tank and a fixed bed column. Ciência & Tecnologia dos Materiais. 2017;29:e229-e233.DOI: 10.1016/j.ctmat.2016.06.009.
63. Aksu Z ,Gönen F. Biosorption of phenol by immobilized activated sludge in a continuous packed bed: prediction of breakthrough curves. Process biochemistry. 2004;39:599-613.
64. Karunarathne H ,Amarasinghe B. Fixed bed adsorption column studies for the removal of aqueous phenol from activated carbon prepared from sugarcane bagasse. Energy Procedia. 2013;34:83-90.
65. Ajmani A, Patra C, Subbiah S, Narayanasamy S. Packed bed column studies of hexavalent chromium adsorption by zinc chloride activated carbon synthesized from Phanera vahlii fruit biomass. Journal of Environmental Chemical Engineering. 2020:103825.
66. Li Y, Zhu Y, Zhu Z, Zhang X, Wang D, Xie L. Fixed-bed column adsorption of arsenic (V) by porous composite of magnetite/hematite/carbon with eucalyptus wood microstructure. Journal of Environmental Engineering and Landscape Management. 2018;26:38-56.

858 **Table 8** Kinetics parameters obtained via linear regression analysis

Model Parameters	**Flow rate (Q, ml/min)**			**Influent conc. (C_o, mg/l)**			**Bed height (Z, cm)**			**Particle size (µm)**		
	9	**13**	**18**	**100**	**200**	**300**	**5**	**7.5**	**10**	**300**	**600**	**800**
Thomas												
K_{TH}	0.000934	0.00128	0.00252	0.000817	0.000383	0.000429	0.00273	0.00175	0.00239	0.00151	0.00267	0.00474
q_{TH}	6.509	3.391	1.710	5.357	2.746	2.039	3.065	6.664	8.026	7.232	3.832	2.119
R^2	0.9800	0.9540	0.9900	0.9720	0.9770	0.8940	0.9650	0.9710	0.9700	0.9880	0.9700	0.8910
Adam-Bohart												
K_{AB}	0.00055	0.000516	0.00071	0.000441	0.000125	0.000057	0.00060	0.00879	0.00233	0.00101	0.00055	0.00034
N_o	1416.873	1484.112	1571.553	1483.693	2645.885	2621.981	2985.34	1818.998	908.081	1157.675	861.021	769.845
R^2	0.9880	0.9940	0.8840	0.9850	0.9850	0.9830	0.8810	0.9730	0.9270	0.9770	0.9600	0.9020
Wolborska												
β	0.7793	0.7658	0.7402	0.6543	0.3307	0.1486	1.7882	1.5989	2.1186	1.1704	0.9084	0.4881
N_o	1416.873	1484.112	1571.553	1483.693	2645.885	2621.981	2985.34	1818.998	908.081	1157.675	861.0208	769.845
R^2	0.9880	0.9940	0.8840	0.9850	0.9850	0.9830	0.8810	0.9730	0.9270	0.9770	0.9600	0.9020
Yoon Nelson												
K_{YN}	0.0961	0.1584	0.3474	0.082	0.082	0.285	0.2733	0.1755	0.239	0.146	0.256	0.447

τ	11.87	4.542	2.6327	9.951	2.000	0.908	2.84	9.25	14.86	13.5	6.933	3.496
	41						2	1		2		
R^2	0.985	0.939	0.8980	0.984	0.984	0.670	0.96	0.97	0.970	0.98	0.965	0.8830
	0	0		0	0	0	50	10	0	40	0	

859

860

861 **Table 9** Kinetics parameters obtained via nonlinear regression analysis

Model	**Flow rate**			**Influent conc. (C_o,**			**Bed height**			**Particle size (μm)**		
Parameters	**(Q, ml/min)**			**mg/l)**			**(Z, cm)**					
	9	**13**	**18**	**100**	**200**	**300**	**5**	**7.5**	**10**	**300**	**600**	**800**
Thomas												
K_{TH}	0.000	0.000	0.0048	0.000	0.008	0.001	0.00	0.001	0.001	0.00	0.002	0.003
	665	711	577	463	999	878	610	87	797	1228	024	062
q_{TH}	8.659	4.623	3.404	8.207	5.060	3.526	4.16	7.042	8.685	8.64	4.013	1.881
							5			7		
R^2	1.000	0.992	1.0000	1.000	1.000	1.000	1.00	0.986	0.990	1.00	0.999	1.000
	0	4		0	0	0	00	1	7	00	8	0
RMSE	0.009	0.016	0.0174	0.011	0.060	0.021	0.02	0.007	0.008	0.01	0.005	0.006
	8	4		2	9	0	46	0	3	19	2	8
χ^2	0.008	0.011	0.0064	0.010	0.077	0.006	0.01	0.000	0.011	0.01	0.001	0.000
	9	0		7	4	3	16	3	6	54	0	0
SSE	0.003	0.008	0.0046	0.005	0.072	0.004	0.00	0.000	0.002	0.00	0.000	0.000
	9	8		5	8	7	81	1	3	48	8	1
SAE	0.073	0.134	0.0497	0.087	0.244	0.044	0.08	0.011	0.053	0.07	0.036	0.024
	4	1		5	2	2	84	8	3	81	2	3

ARE	0.5825	1.0018	0.0714	0.7098	1.1728	0.0414	0.3227	0.2979	0.1552	0.5263	0.3291	0.1464
Adam-Bohart												
K_{AB}	0.000540	0.00052	0.000416	0.000449	0.000124	0.000058	0.00057	0.000879	0.002301	0.00102	0.00102	0.00063
N_o	1492.339	1501.015	1511.113	1506.394	2645.554	2698.763	2765.086	1818.055	889.782	1173.932	822.766	730.256
R^2	0.9998	1.0000	0.9999	1.0000	1.0000	1.0000	1.0000	1.0000	1.0000	1.0000	1.0000	1.0000
RMSE	0.0069	0.0021	0.0049	0.0046	0.0020	0.0021	0.0008	0.0078	0.0075	0.0093	0.0054	0.0048
χ^2	0.0038	0.00002	0.00016	0.0016	0.0000	0.0000	0.0004	0.0009	0.0022	0.0077	0.0022	0.0019
SSE	0.0013	0.0000	0.00005	0.0001	0.0000	0.0000	0.0019	0.0004	0.0003	0.0016	0.0000	0.0000
SAE	0.0382	0.0140	0.01504	0.0244	0.0034	0.0140	0.0916	0.0076	0.0663	0.0372	0.0332	0.0015
ARE	0.1086	0.0804	0.25483	0.0033	0.0172	0.0860	0.9037	0.4772	3.0339	0.1778	0.5940	0.4055
Wolborska												
β	0.8074	0.7926	0.64649	0.6779	0.3288	0.1562	0.5967	1.1169	2.0435	1.2014	0.8395	0.4560
N_o	1429.789	1499.792	1501.917	1496.469	2641.706	2687.956	2554.529	1676.702	893.254	1167.76	828.449	739.796
R^2	1.0000	0.9995	0.99910	1.0000	1.0000	1.0000	1.0000	1.0000	1.0000	1.0000	1.0000	1.0000

RMSE	0.005	0.003	0.0053	0.004	0.001	0.002	0.02	0.015	0.007	0.00	0.006	0.005
	3	0		5	9	2	34	8	7	91	0	6
χ^2	0.002	0.000	0.0002	0.001	0.000	0.000	0.01	0.011	0.002	0.00	0.000	0.002
	2	0		5	0	0	92	5	5	74	4	5
SSE	0.000	0.000	0.0000	0.000	0.000	0.000	0.01	0.007	0.000	0.00	0.000	0.000
	6	0		5	1	0	66	1	2	15	0	1
SAE	0.025	0.017	0.0166	0.023	0.003	0.013	0.11	0.075	0.062	0.03	0.027	0.010
	5	2		0	7	3	84	1	3	51	3	3
ARE	0.034	0.092	0.2772	0.011	0.019	0.081	0.52	0.397	2.944	0.20	0.544	0.346
	5	6		8	1	9	62	3	6	83	6	9
Yoon Nelson												
K_{YN}	0.061	0.185	0.2395	0.065	0.066	0.209	0.21	0.138	0.189	0.17	0.227	0.342
	3	3		5	7	9	27	7	8	78	9	7
τ	11.84	5.926	1.0316	9.998	2.056	0.503	2.99	9.786	15.73	14.5	7.082	3.764
	08	4		5	2	6	63	5	62	592	6	5
R^2	0.975	1.000	1.0000	0.996	0.995	0.995	1.00	0.999	0.999	0.99	1.000	1.000
	4	0		1	9	3	00	9	5	93	0	0
RMSE	0.017	0.011	0.0937	0.001	0.193	0.303	0.38	0.018	0.014	0.03	0.006	0.451
	7	8		7	2	1	04	9	7	69	6	2
χ^2	0.001	0.032	0.0605	0.001	0.471	0.952	1.17	0.004	0.031	0.09	0.002	0.133
	7	1		2	3	2	35	5	0	50	6	8
SSE	0.000	0.165	0.5487	0.001	0.791	9.919	10.4	0.015	0.009	0.03	0.007	8.526
	8	6		7	0	7	487	7	2	71	3	0
SAE	0.017	0.231	1.0117	0.085	1.154	8.612	2.70	0.083	0.114	0.20	0.032	4.752
	4	2		1	1	6	75	3	9	85	0	3
ARE	0.030	0.103	2.4203	0.198	1.944	2.358	1.09	0.065	0.065	0.36	0.904	5.606
	3	0		4	3	1	12	8	7	38	0	9

862

Figures

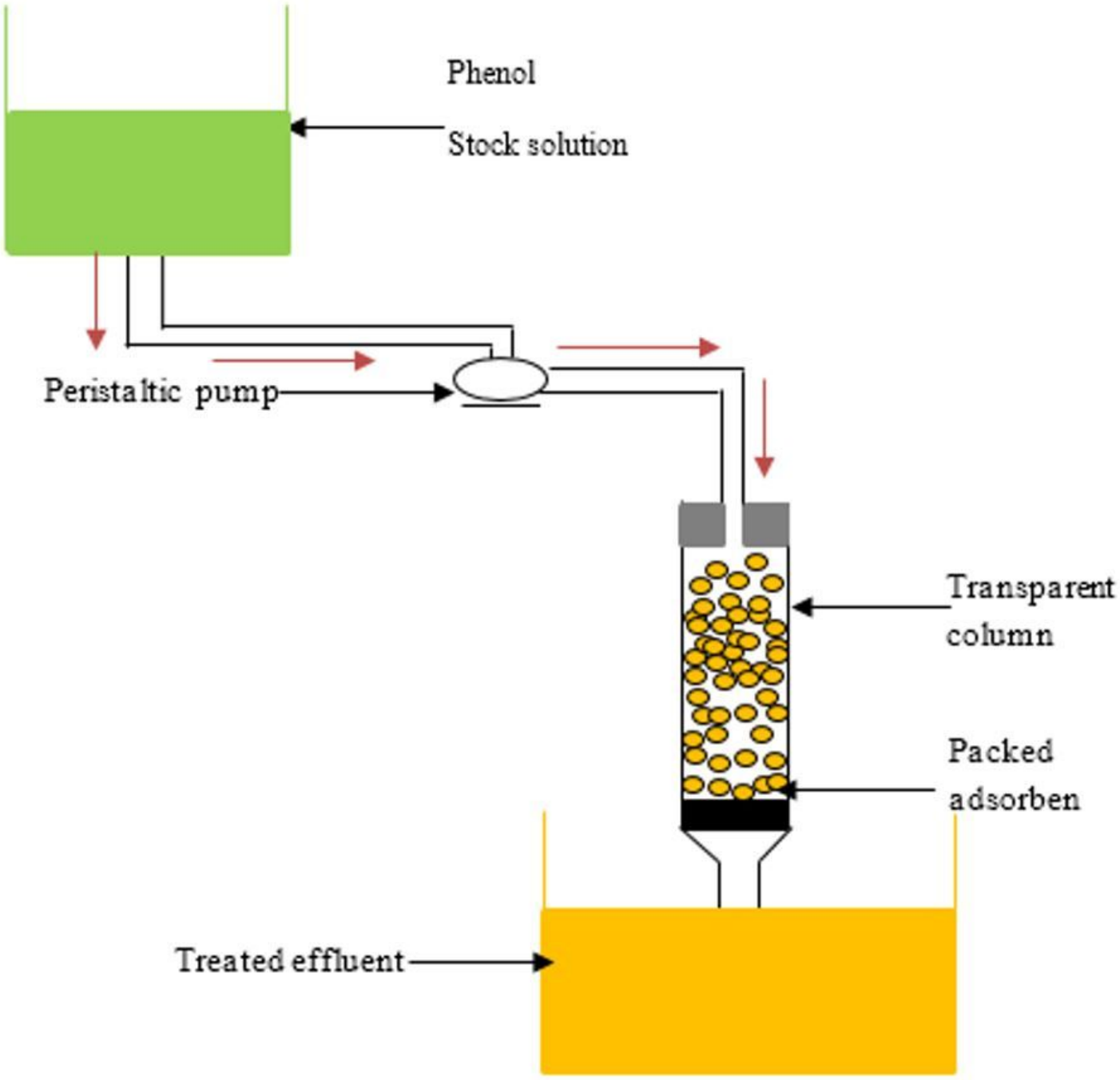

Figure 1

Packed bed column experimental set up

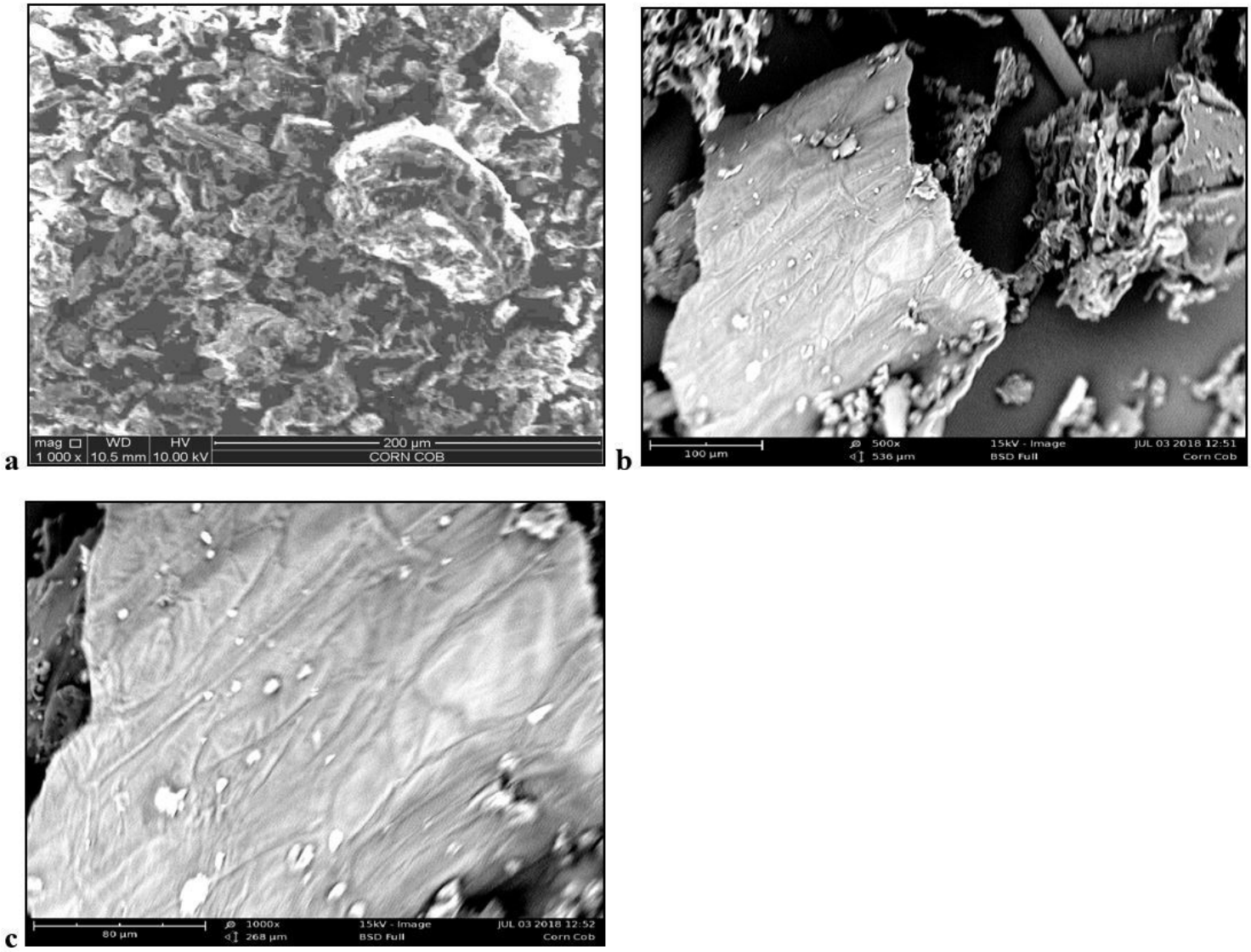

Figure 2

SEM images of (a) raw corn at 500x, (b) CCAC at 500x, (c) CCAC at 1000x.

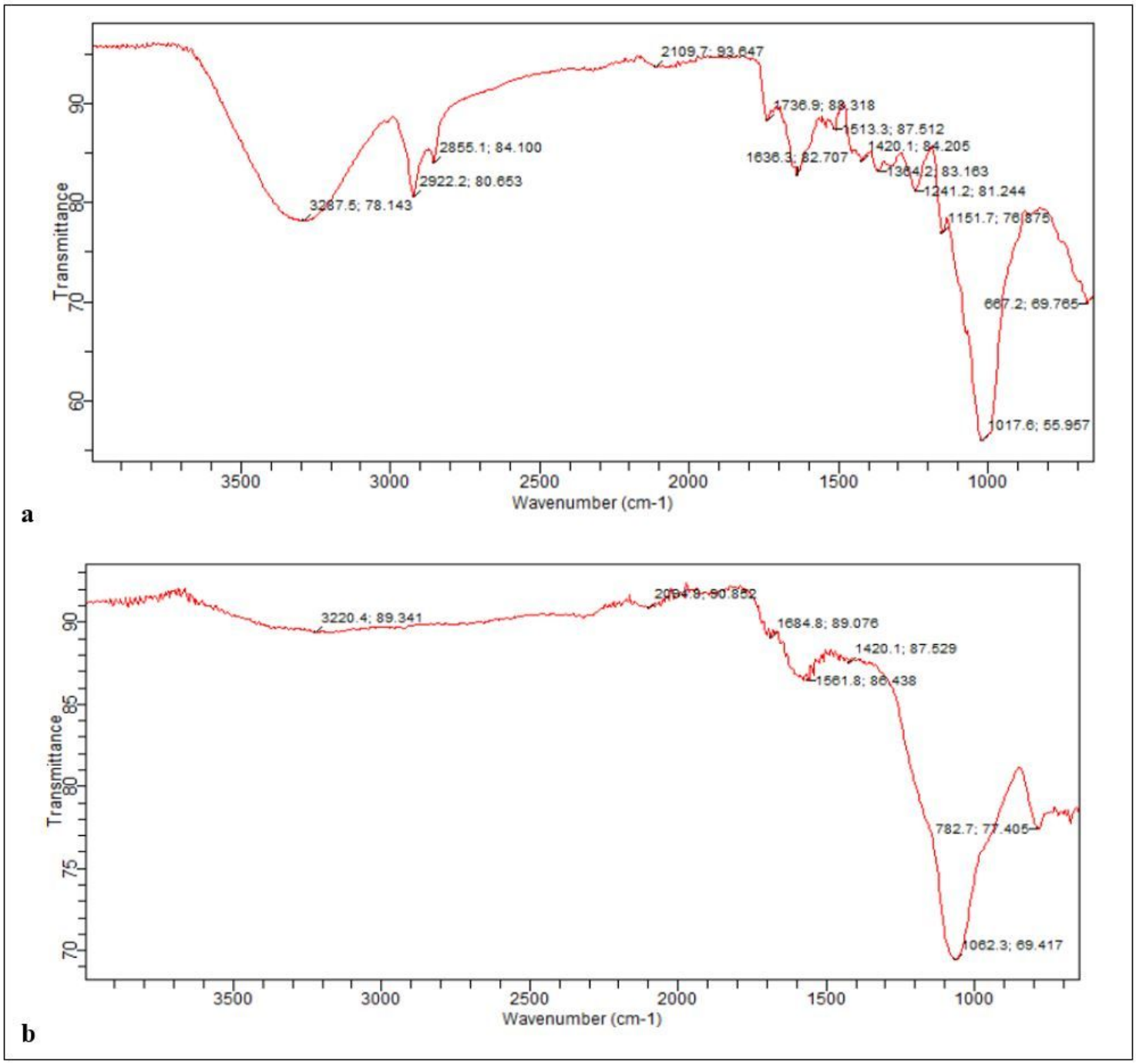

Figure 3

FTIR spectrum of (a) raw corn cob; (b) CCAC

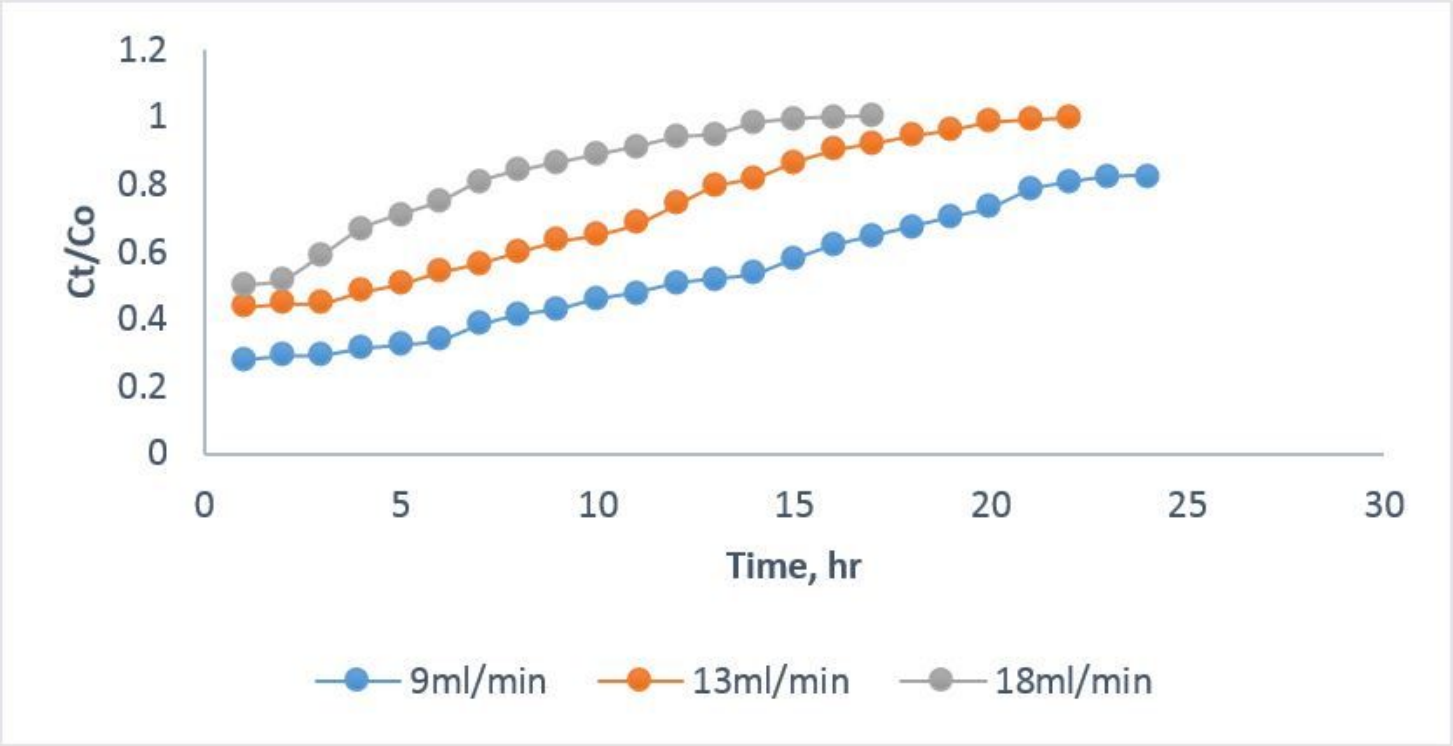

Figure 4

Effect of flowrate on the breakthrough curve

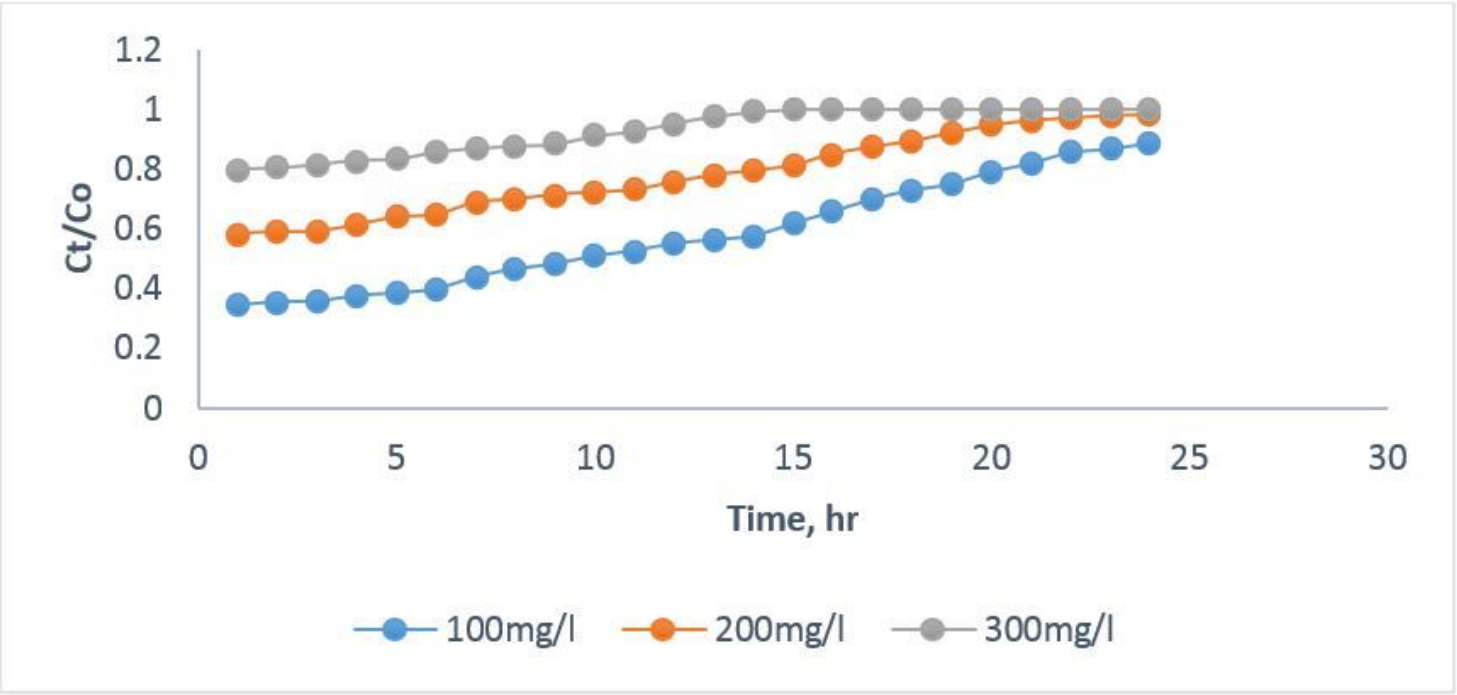

Figure 5

Effect of influent concentration on the breakthrough curve

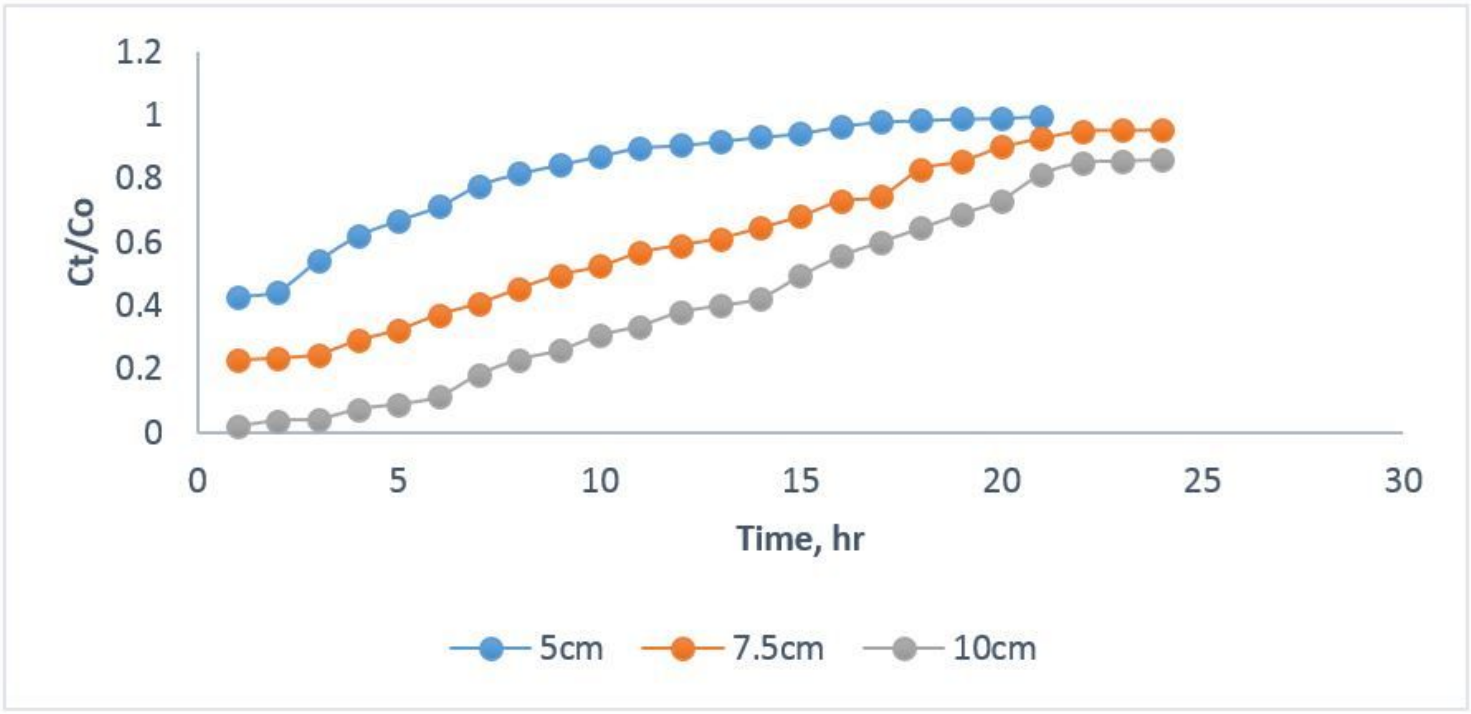

Figure 6

Effect of bed height on the breakthrough curve

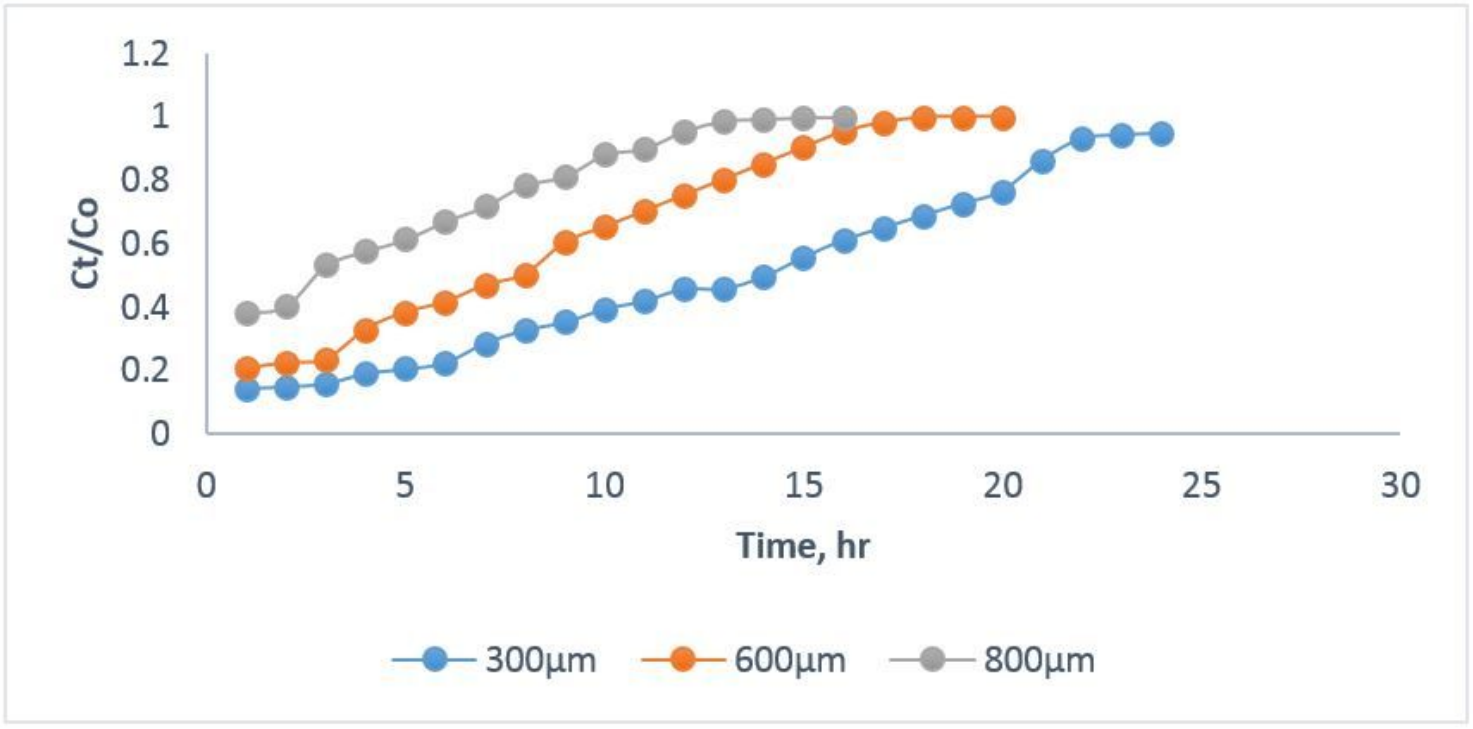

Figure 7

Effect of particle size on the breakthrough curve

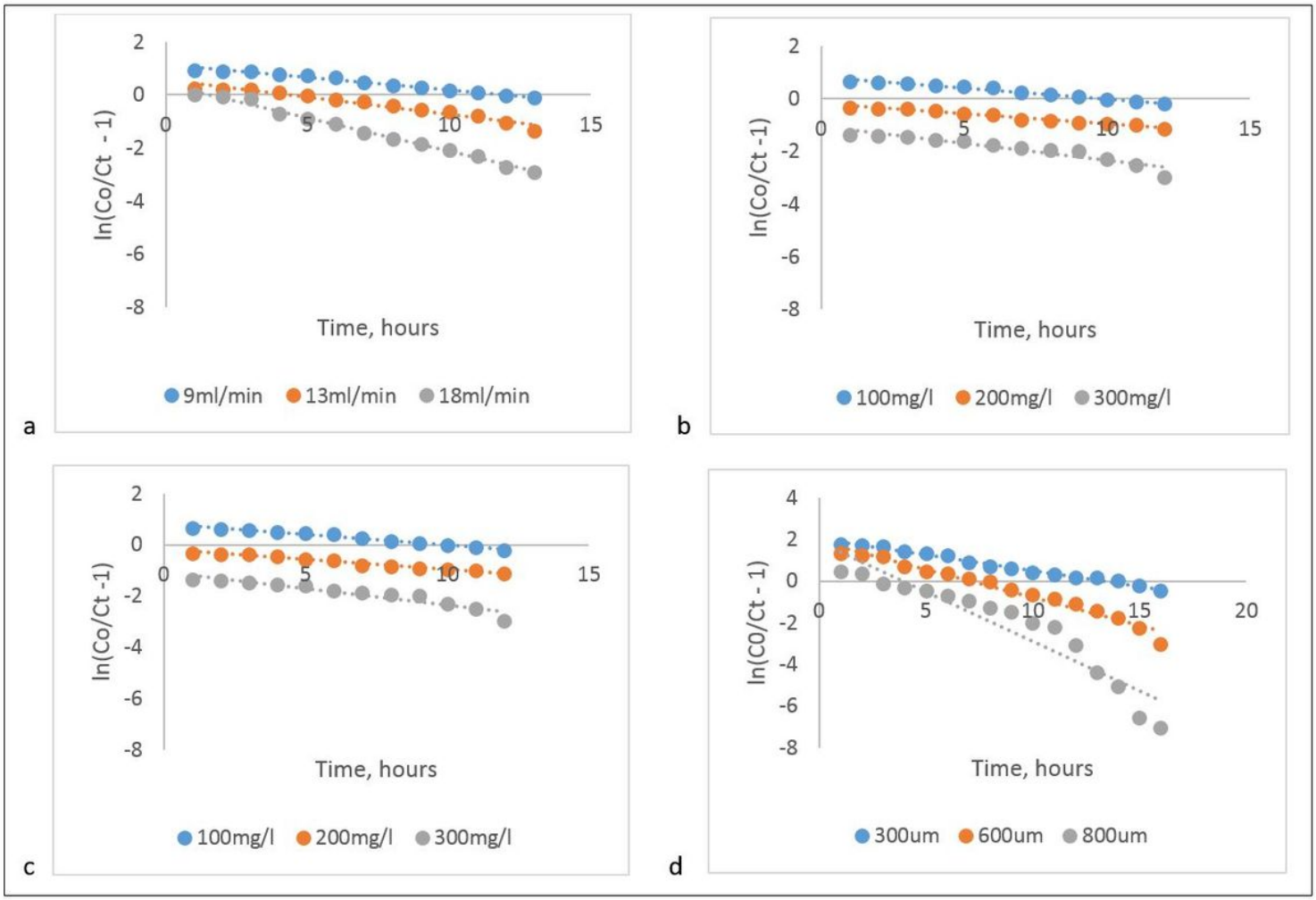

Figure 8

Linear plots of Thomas kinetic model: (a) at different flow rates; (b) at different influent concentration (c) at different bed heights; (d) at different particle sizes

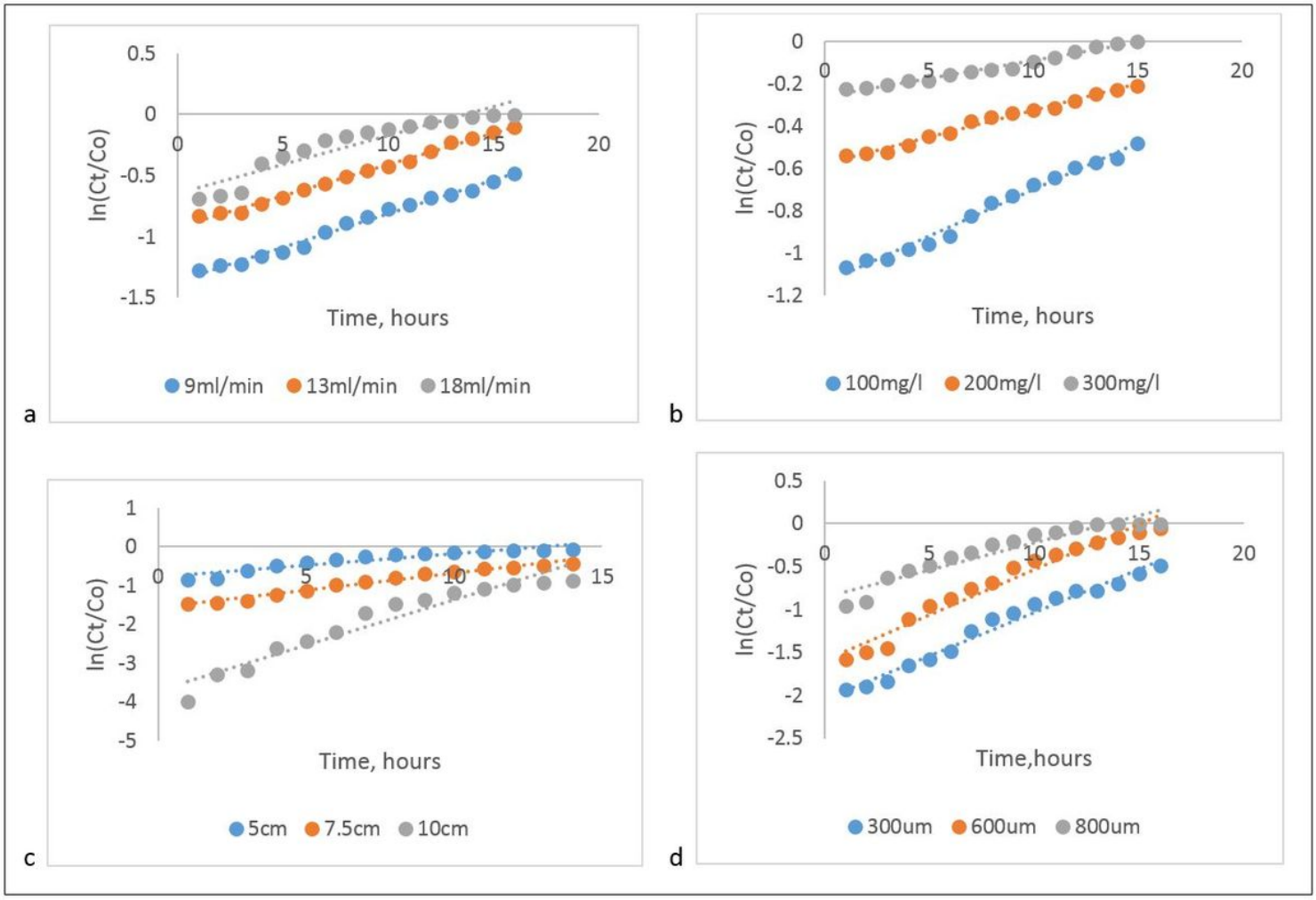

Figure 9

Linear plots of Adam-Bohart kinetic model: (a) at different flow rates; (b) at different influent concentration; (c) at different bed heights; (d) at different particle size

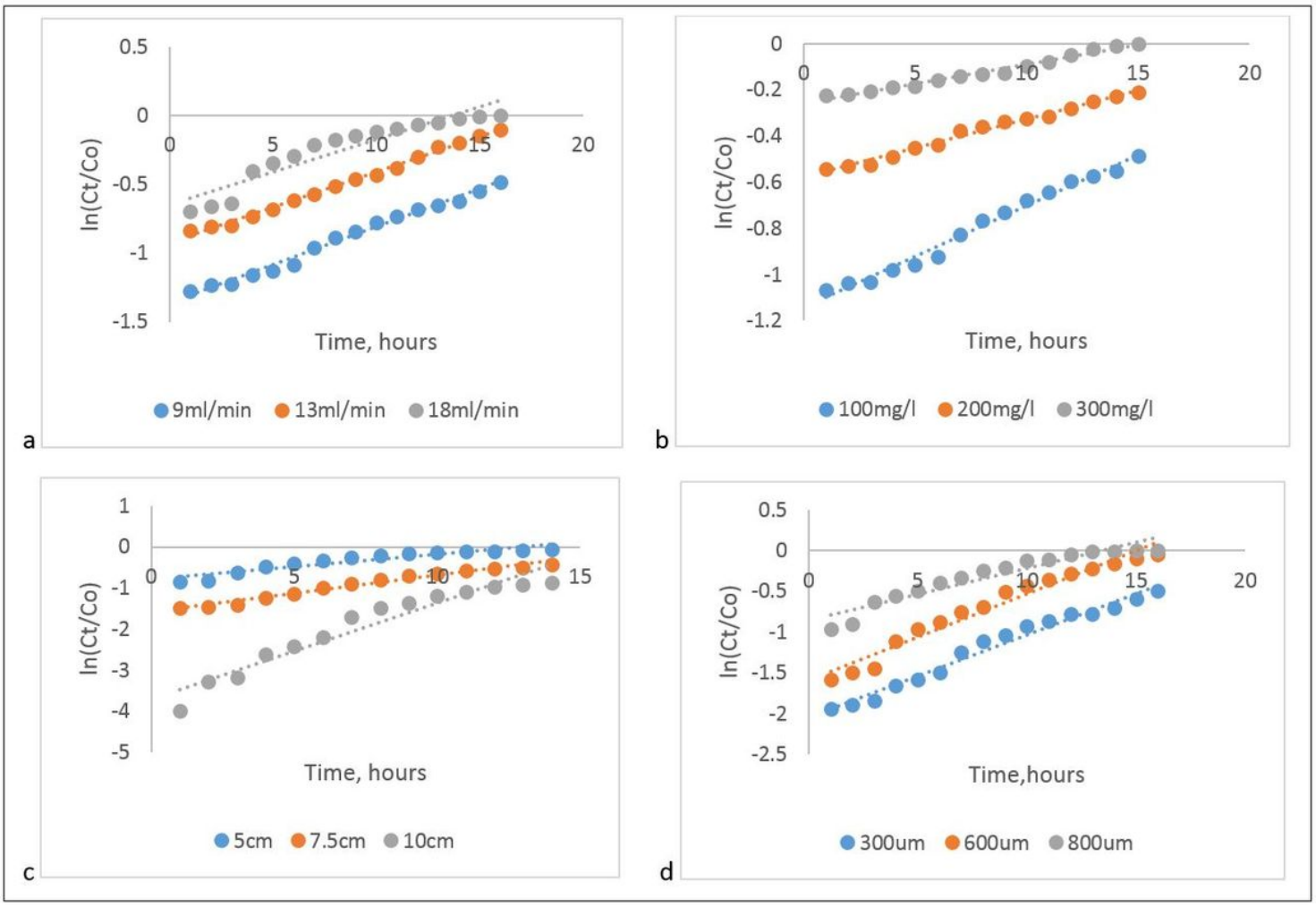

Figure 10

Linear plots of Wolborska kinetic model: (a) at different flow rates; (b) at different influent concentration; (c) at different bed heights; (d) at different particle size

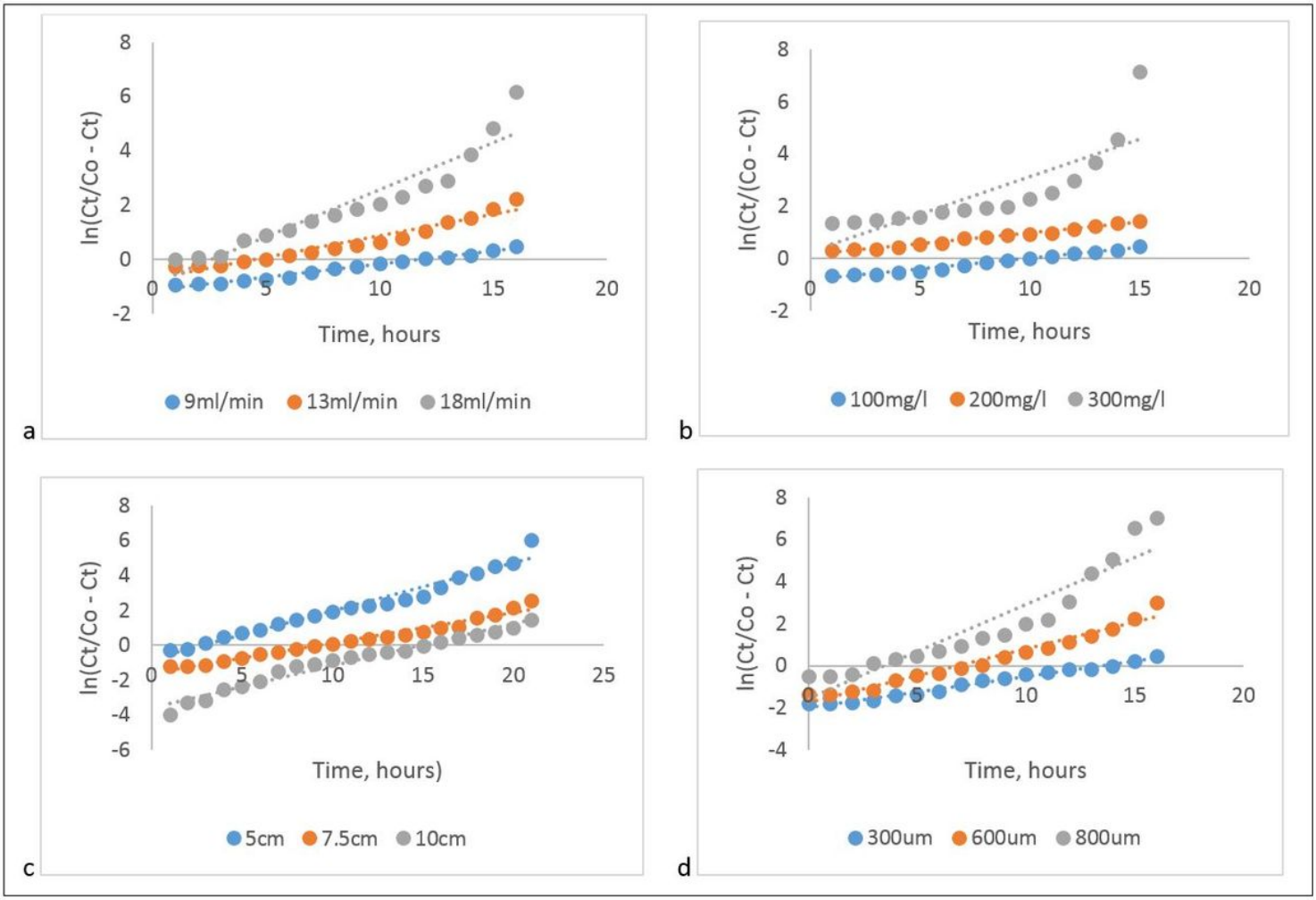

Figure 11

Linear plots of Yoon-Nelson kinetic model: (a) at different flow rates; (b) at different influent concentrations; (c) at different bed heights; (d) at different particle sizes